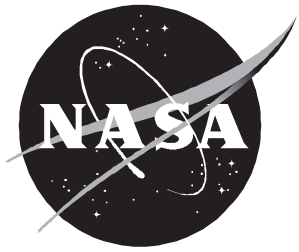

NASA Technical Memorandum 4634
ATCOM Technical Report 95-A-001

Exploratory Flow Visualization Investigation of Mast-Mounted Sights in Presence of a Rotor

Terence A. Ghee and Henry L. Kelley

March 1995

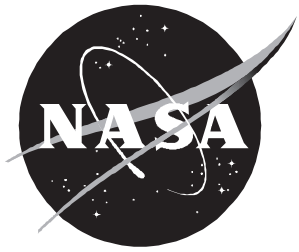

NASA Technical Memorandum 4634
ATCOM Technical Report 95-A-001

Exploratory Flow Visualization Investigation of Mast-Mounted Sights in Presence of a Rotor

Terence A. Ghee
Analytical Services & Materials, Inc. • Hampton, Virginia

Henry L. Kelley
Joint Research Program Office
Aeroflightdynamics Directorate
U.S. Army Aviation and Troop Command
Langley Research Center • Hampton, Virginia

National Aeronautics and Space Administration
Langley Research Center • Hampton, Virginia 23681-0001

March 1995

Available electronically at the following URL address: http://techreports.larc.nasa.gov/ltrs/ltrs.html

Printed copies available from the following:

NASA Center for AeroSpace Information
800 Elkridge Landing Road
Linthicum Heights, MD 21090-2934
(301) 621-0390

National Technical Information Service (NTIS)
5285 Port Royal Road
Springfield, VA 22161-2171
(703) 487-4650

Contents

Tables

Figures

Abstract

A flow visualization investigation with a laser light sheet system was conducted on a 27-percent-scale AH-64 attack helicopter model fitted with two mast-mounted sights in the Langley 14- by 22-Foot Subsonic Tunnel. The investigation was conducted to identify aerodynamic phenomena that may have contributed to adverse vibration encountered during full-scale flight of the AH-64D Apache/Longbow helicopter with an asymmetric mast-mounted sight. Symmetric and asymmetric mast-mounted sights oriented at several skew angles were tested at simulated forward and rearward flight speeds of 30 and 45 knots. A laser light sheet system was used to visualize the flow in planes parallel to and perpendicular to the free-stream flow. Analysis of these flow visualization data identified frequencies of flow patterns in the wake shed from the sight, the streamline angle at the sight, and the location where the shed wake crossed the rotor plane. Differences in wake structure were observed between the sight configurations and various skew angles. Analysis of lateral light sheet plane data implied significant vortex structure in the wake of the asymmetric mast-mounted sight in the configuration that produced maximum in-flight vibration. The data showed no significant vortex structure in the wake of the asymmetric and symmetric configurations that produced no increase in in-flight adverse vibration.

Introduction

During recent industry development flight testing on an AH-64D Apache/Longbow attack helicopter equipped with an asymmetric mast-mounted sight (AMMS), severe vibration was encountered during certain rearward flight conditions. (See fig. 1.) Previous testing on the aircraft with a symmetric mast-mounted sight (SMMS) revealed no adverse vibration problem. The government and industry team conducting the flight tests proposed the following aerodynamic explanations of the adverse vibration:

1. Wake shed from the AMMS produced unsteady aerodynamic forces on the sight that caused the main rotor shaft to vibrate.

2. Wake shed from the AMMS passed through the plane of the main rotor and created a change in the local angle of attack of the main rotor blades that resulted in an impulsive blade lift distribution and increased rotor vibration.

3. Wake shed from the AMMS passed through the plane of the main rotor and impinged on the fuselage, which resulted in unsteady pressure forces on the fuselage.

4. The fuselage orientation, in conjunction with certain AMMS configurations, caused a change in the flow structure upstream of the sight that caused differences in the wake downstream of the sight. The vibration could occur in a manner similar to explanation 2 or 3.

To understand the aerodynamic interactions between a mast-mounted sight and a rotor-fuselage configuration, tests were conducted on models of the AH-64 equipped with and without mast-mounted sights (MMS) in the Langley 14- by 22-Foot Subsonic Tunnel. Three model configurations were investigated: (1) the AH-64 without an MMS, (2) the AH-64 with an AMMS, and (3) the AH-64 with an SMMS. Tests were conducted at a rotor thrust coefficient representative of a full-scale gross weight of 16 500 lb in simulated forward and rearward flight at tunnel velocities of 30 and 45 knots. However, without dynamic similarity of the rotor and fuselage structure, actual in-flight vibration problems were impossible to address during this investigation. A laser light sheet system was used to obtain flow visualization in the vicinity of the model to highlight aerodynamic phenomena that may have contributed to the vibration problem.

Symbols

AMMS	asymmetric mast-mounted sight
c_e	thrust-weighted equivalent blade chord, ft
C_T	rotor thrust coefficient, $\frac{T}{\rho\pi\Omega^2 R^4}$
d	chord length of mast-mounted sight, ft
f	sight-wake shedding frequency, Hz
GRMS	General Rotor Model System
MMS	mast-mounted sight
r	rotor radial location (measured from rotor hub center), ft
$\bar{r}$	mean rotor radial location, ft

R	rotor radius, 6.48 ft
Re	Reynolds number, $\frac{\rho_\infty V_\infty d}{\mu_\infty}$
SMMS	symmetric mast-mounted sight
St	Strouhal number, $\frac{tf}{V_\infty}$
t	thickness of mast-mounted sight, ft
T	rotor thrust, lb
V_∞	free-stream velocity, ft/s
x	downstream distance (measured from rotor hub center), ft
y	lateral distance (measured from rotor hub center), ft
α_s	shaft angle (negative inclined forward), deg
α_{TPP}	angle of attack of tip path plane (negative inclined forward), deg
β	skew angle of mast-mounted sight, deg
λ	sight-wake wavelength, ft
μ	advance ratio, $V_\infty \cos\frac{\alpha_{TPP}}{\Omega R}$
μ_∞	viscosity $\approx 3.7373 \times 10^{-7}$ slug/ft
ρ_∞	density of free-stream flow, slug/ft^3
σ_{th}	thrust-weighted solidity, $4c_e/\pi R$
ψ	rotor azimuth angle, deg
Ω	rotor rotational frequency, rad/s

Experimental Apparatus

The investigation was performed in the Langley 14- by 22-Foot Subsonic Tunnel (ref. 1). A laser light sheet system was used to visualize the flow. The experimental model hardware included the following: (1) NASA/ Army General Rotor Model System (GRMS), which is described in reference 2, (2) 27-percent-scale rotor hub, dynamically scaled from the AH-64 hub, (3) 27-percent-scale advanced-geometry (3:1 taper ratio) rotor blades dynamically scale from the AH-64 main rotor blade, (4) 27-percent-scale AH-64 model fuselage shell used for the forward flight portion of the investigation, (5) 30-percent-scale AH-64 model fuselage shell used for the rearward flight portion of the investigation, and (6) 27-percent-scale symmetric and asymmetric mast-mounted sights, both scaled geometrically (figs. 2 and 3). The test facility, laser light sheet system, and model hardware are described in the following paragraphs.

The Langley 14- by 22-Foot Subsonic Tunnel is a closed-circuit, low-speed, atmospheric wind tunnel designed for testing V/STOL (vertical/short takeoff and landing) models. (See fig. 4.) This facility can operate in a partially open test section configuration by lifting the walls and ceiling. For this investigation, the open test section configuration was used to allow maximum optical access to the sight and rotor wakes and minimize wall interference at low speeds. The tunnel data acquisition system provided tunnel operating conditions and model parameter measurements. The data reduction procedure included wind tunnel wall effect corrections to the tunnel dynamic pressure and flow angularity (ref. 3).

A laser light sheet system was used in conjunction with smoke injected into the tunnel free stream to provide flow visualization near the rotor system and the sights. The vaporized propylene glycol smoke was injected into the air stream in the tunnel settling chamber, approximately 90 ft upstream of the tunnel test section. The smoke generator was mounted on a traversing rig, which was moved horizontally and vertically to allow the plume of smoke to be positioned in the test section. The system used an argon ion laser that produced a 5-W beam. This beam was directed through a Bragg cell (acousto-optical modulator) and then through a length of fiber-optic cable to a cylindrical lens that created the light sheet. Figure 5 is a schematic diagram of this system. The light sheet position was varied by rotating a mirror located in-line with the cylindrical lens. The light sheet could be pulsed with the Bragg cell that was triggered by the once-per-revolution signal from the main rotor shaft encoder or by a signal from a function generator. Both triggering methods were used during the test program to “freeze” the rotor-sight wake (ref. 4). The flow structure in the plane of the laser light sheet was made visible by the propylene glycol smoke (ref. 5).

The GRMS is a fully instrumented rotor drive and control system that can be configured for a wide variety of rotors (refs. 2 and 6) and consists of two 90-hp electric motors, a transmission, and cyclic and collective controls. Figure 6 is a sketch of the GRMS with the 27-percent-scale fuselage used in forward flight with an MMS installed. A digital encoder was used to measure rotor RPM and provide a rotor azimuthal reference. This azimuthal reference was also used to derive a trigger for the laser light sheet. In addition, blade flapping, lagging, feathering, and cyclic and collective control angles were monitored and recorded.

The AH-64 model hub was dynamically scaled and duplicated the major features of the full-scale AH-64 hub (ref. 7). The hub was fully articulated and featured a multilayered strap retention system located inside the pitch cases with elastomeric lead-lag dampers located on either side of the pitch cases. The straps inside the pitch housing flexed to allow feathering and flapping of the blade. As with the full-scale hub, the lead-lag motion of the blade took place through a fitting that was mounted at

the outboard end of the pitch cases and connected the pitch case, retention straps, blade, and lead-lag dampers.

Figure 7 shows a plan view of the advanced rotor (3:1 taper ratio) model blade and a sketch of the scaled baseline blade of the AH-64. The baseline blades were damaged during an earlier test and were not available. The blade used for the present investigation was used in a previous study (ref. 8). The blade had a linear twist of −12°, an inboard chord of 7.17 in., and a 3:1 planform taper from $r/R = 0.8$ to the tip. Three airfoil sections developed at Langley for rotorcraft application were used on the rotor: RC(3)-10, RC(3)-08, and modified RC(3)-10. The data for the NASA RC(3)-10 and RC(3)-08 airfoils are presented in reference 9. The modification for the RC(3)-10 airfoil was a raised camberline. The advanced rotor blade had the same diameter and had the same thrust weighted solidity as the baseline blade.

The model blades were fabricated from composite materials to meet the demanding requirements of dynamic similarity and Mach scaling. An effort was made to preserve the full-scale dynamic properties in the model blades; however, these properties were difficult to maintain in the tip region because of tip taper. The combined limitations imposed by taper and scale resulted in insufficient volume at the tip; thus the mass and stiffness characteristics of the full-scale baseline rotor could not be accurately modeled (ref. 8). The dimensional accuracy of the blade set contours was held to 0.005 in., and the blade surface smoothness was measured to be 0.0008 to 0.0012 in.

The shells that modeled the AH-64 fuselage were made from fiberglass epoxy. The shell used during forward flight testing was a 27-percent scale. Rearward flight simulation was complicated by the fact that the 27-percent-scale shell was too small to mount backwards on the GRMS and because the sting could not be yawed greater than ±45°. A 30-percent-scale shell was available from a previous investigation and was used during the rearward flight portion of this investigation. The 30-percent-scale shell could not be adjusted to model the shaft tilt of 5° relative to the fuselage and was set at 0°. Although the rearward flight simulation included these differences, the overall flow field was believed to be sufficiently modeled to provide insight into potential rotor, wake, and body aerodynamic interactions. Figures 8 and 9 show the forward and rearward fuselage shells mounted in the tunnel.

The models did not include the horizontal and vertical tails. Furthermore, to accommodate the sting mount for the 30-percent-scale shell (rearward flight), a small section of the nose was cut away. Pylons, missile racks, missiles, and landing gear were not installed on the rearward flight shell but were included during testing of the forward flight shell. These differences between the forward and rearward flight configurations were not felt to have a significant effect on the aerodynamics of the MMS. Both shells included wings (stores carriers), but engine inlet flow and exhaust were not modeled for either shell. The 27-percent-scale shell was mounted on a six-component strain-gauge balance. Because of mounting constraints, the 30-percent-scale shell was not mounted on a balance.

Both the symmetric and the asymmetric mast-mounted sights were made of fiberglass epoxy and were geometrically (but not dynamically) scaled 27 percent to the full-scale sights. These sights were mounted to the hub with hardware adopted from a previous study. Figure 10 shows the sight components, and figure 11 shows the sign convention of the AMMS skew angle and rotor system.

Test Procedure and Data Processing

A limited test matrix was selected because the full-scale helicopter with AMMS was known to experience severe vibration only over a narrow portion of the flight envelope. Tests were conducted at advance ratios, $\mu = 0.07$ and 0.10, which correspond to tunnel flow velocities of 30 and 45 knots, respectively. Although testing in the flight range of 15 to 30 knots was desirable to duplicate all flight test conditions, lower tunnel velocities were not feasible because of uncertainties in large dynamic pressure and angle-of-attack corrections that were caused by the large model rotor operating at low speed and high thrust. For both fuselage models, the angle of attack of the shaft was fixed at 0° and a constant rotor thrust coefficient ($C_T = 0.0072$) was maintained to correspond to a full-scale vehicle weight of 16500 lb. The angle of attack of the shaft α_s was not varied because of time constraints and because only small changes in α_s were required to trim the full-scale vehicle at forward flight speeds of 45 knots ($\alpha = 0.5°$) and 30 knots ($\alpha = -0.2°$). (See ref. 10.)

The fuselage tilt for the forward flight model was set at 5° nose up (same as the full-scale vehicle). The rearward flight model was set at fuselage tilt of 0° because of physical mounting constraints. The main rotor RPM was reduced from 1070 to 900 to maintain the desired thrust coefficient at modest electric drive motor power levels to minimize the possibility of motor overheating. This reduction in RPM reduced the blade tip Mach number from the full-scale sea-level value of 0.63 to 0.53.

Table 1 and figure 12 show the test matrix and the configurations used in the investigation, respectively. The following nine configurations were tested: baseline (no sight, configuration 1), symmetric mast-mounted sight in forward and rearward flight (configurations 2

Table 1. Test Matrix

[Configuration numbers from fig.12]

Configuration	μ	Test condition	Light sheet orientation
4	0.07	AMMS, forward flight, –30°	Longitudinal
6		AMMS, forward flight, 180°	Longitudinal
2		SMMS, forward flight	Longitudinal
7		AMMS, rearward flight, –30°	Both
9		AMMS, rearward flight, 180°	Lateral
8		AMMS, rearward flight, 0°	Longitudinal
3		SMMS, rearward flight	Lateral
4	0.10	AMMS, forward flight, –30°	Longitudinal
6		AMMS, forward flight, 180°	Longitudinal
2		SMMS, forward flight	Longitudinal
7		AMMS, rearward flight, –30°	Both
9		AMMS, rearward flight, 180°	Lateral
8		AMMS, rearward flight, 0°	Longitudinal
3		SMMS, rearward flight	Lateral

and 3), asymmetric mast-mounted sight in forward flight with the sight oriented at skew angles of $\beta = -30°$, 0°, and 180° with respect to the free-stream velocity (configurations 4, 5, and 6), and asymmetric mast-mounted sight in rearward flight with the sight oriented at skew angles of $\beta = -30°$, 0°, and 180° with respect to the free-stream velocity (configurations 7, 8, and 9). The skew angle β for the AMMS is defined as the angle formed in the horizontal plane between the free-stream tunnel velocity and the blunt face of the AMMS (fig. 11). Positive sight skew angles have a counterclockwise rotation when the sight is viewed from above. Only configurations 7 and 8 experienced adverse vibration in the full-scale flight tests; configuration 7 experienced the most severe vibration.

The light sheet plane was positioned either perpendicular or parallel to the free-stream velocity. The longitudinal (parallel to the free stream) light sheet position included the center of the sight and along both edges of the sight (lateral distance from the model centerline (y/R) of 0.00 and approximately ±0.15), which allowed the coherent vortex shed from the sight to be visualized. (See fig. 13.) The lateral (perpendicular to the free stream) light sheet locations included numerous positions upstream of the sight, on the sight, and downstream of the sight (downstream locations relative to the hub center (x/R) of approximately ±0.25, ±0.15, 0.00, 0.30, and 0.35). (See fig. 14.) Using a lateral light sheet permitted the trailed vorticity shed from the edges of the sight to be visualized. At each test condition, data consisted of strobed and continuous light sheet video recording.

Video recordings of the laser light sheet images were acquired after the AH-64 model rotor and tunnel velocities were stabilized at the desired test condition. These images were collected with a high-resolution video camera (≈700 lines of vertical resolution) and video recorder (≈500 lines of vertical resolution). For the longitudinal light sheet planes, a reference grid was placed in the plane of the light sheet and videotaped with the tunnel and rotor system shut down. The camera settings were kept identical between a series of data and reference images. The lateral light sheet plane images were qualified by comparing the wake structure for different sight configurations; hence, the reference grid necessary for longitudinal light sheet analysis was not used.

The video images on the tape were selectively digitized and stored on a computer hard disk. To bring out salient flow features, the data were enhanced with traditional image processing techniques, that is, adjustment of contrast, histogram stretching, and pseudocoloring (refs. 11 and 12).

After obtaining the best quality image possible through enhancement, the longitudinal light sheet plane image was analyzed. The analysis determined sight-wake and rotor-plane crossing location, mast-mounted-sight streamline angle, and estimates of the sight-wake shedding frequency. This analysis was accomplished by superimposing an image of a reference grid onto the data image to provide a spatial reference. (See fig. 15.) This reference grid, composed of a series of 4-in. by 4-in. squares, was orthogonal to the optical axis of the camera and was placed as close to the rotor hub as physically possible. Thus, estimates of the sight-wake and rotor-plane crossing location and MMS angle of attack could be determined. A measurement software package that gave the precise pixel coordinates of a point on the video image facilitated the data analysis.

The strobing capability of the laser light sheet system permitted the shed wake of the sight to appear stationary. The shedding was not periodic; thus, the frequency could not be determined by strobing the laser sheet in sync with the shed wake. The approximate shedding frequency was calculated by obtaining a single video frame with at least two visible wake periods shed from the sight. Estimates of wake-shedding frequency were determined from

$$f = \frac{V_\infty}{\lambda} \tag{1}$$

where the velocity at the sight was assumed to be the free-stream value. While the assumption of free-stream conditions at the sights is probably not quantitatively precise, it was felt that the shedding frequency of the various configurations could be compared qualitatively on this basis. This frequency was nondimensionalized by computing the Strouhal number as defined by

$$St = \frac{tf}{V_\infty} \tag{2}$$

The shedding frequency and sight-wake and rotor-plane crossing location were unsteady for a given configuration; thus, a statistical approach was undertaken to quantify the data. At least 35 video images from a given configuration were analyzed to determine mean value and standard deviation for shedding frequency and the sight-wake and rotor-plane crossing point.

Uncertainty Analysis

An uncertainty analysis was conducted to determine the accuracy of the video data. The spatial resolution for the video images was approximately 0.15 in. The center of shed vorticity was estimated to be within ±2 pixels, or ±0.30 in. Based on these estimates, the uncertainties of the mean frequency shed from the wake were estimated to be approximately 3.5 and 4.5 percent for advance ratios of 0.07 and 0.10, respectively. The sight-wake and rotor-plane crossing location was estimated to be accurate to ±2 pixels, or an $\bar{r}/R$ of 0.004. The uncertainties in the sight streamline angle were estimated to be 0.06° and 0.20° for advance ratios of 0.07 and 0.10, respectively. The uncertainty in rotor azimuth based upon the resolution of the rotor shaft encoder was 0.35°.

Results

Longitudinal Light Sheet

Figure 16 is a typical video image obtained with the light sheet positioned longitudinally for the AMMS. This image was enhanced with standard image-processing techniques such as histogram stretching and contrast adjustment. However, the image lost some resolution during the conversion process from video to hard copy. Shown in the figure are the wake shed from the sight, an estimate of the sight-wake and rotor-plane crossing location, and an approximate streamline angle at the leading edge of the sight. The wake shed from the sight had the appearance of a Von Karman vortex street shed from a circular cylinder (refs. 13 to 15). The MMS-wake and rotor-plane crossing locations and the shedding frequencies of the sight wake were determined for MMS configurations 3, 4, 7, 8, and 9 (fig. 12) and investigated at both advance ratios with the light sheet centered on the sight. Figure 17 shows the baseline configuration (no MMS) in forward flight.

Table 2 contains the MMS-wake and rotor-plane crossing locations for advance ratios of 0.07 and 0.10. The mean-sight-wake and rotor-plane crossing points were estimated to be $\bar{r}/R = 0.37$ and 0.46 for advance ratios of 0.07 and 0.10, respectively. Significant differences in the MMS-wake and rotor-plane crossing location for the various configurations may support the proposed explanation of the adverse vibration as being the result of blade loading changes. As shown in table 2, for a given advance ratio, little difference was noted in the mean crossing locations for the various configurations, with the greatest difference being only $r/R = 0.06$ at $\mu = 0.07$. Depending on the configuration, the crossing location moved outboard by 5 to 12 percent as the advance ratio was increased. The sight-wake and rotor-plane crossing location results for simulated forward and

Table 2. MMS-Wake and Rotor-Plane Crossing Location

[Configuration numbers from fig.12]

Configuration	μ	Test condition	$\bar{r}/R$	Std. dev.
7	0.07	AMMS, rearward flight, –30°	0.35	0.013
8		AMMS, rearward flight, 0°	.39	.017
4		AMMS, forward flight, –30°	.36	.018
6		AMMS, forward flight, 180°	.41	.020
2		SMMS, forward flight	.37	.022
7	0.10	AMMS, rearward flight, –30°	0.45	0.035
8		AMMS, rearward flight, 0°	.45	.024
4		AMMS, forward flight, –30°	.45	.024
6		AMMS, forward flight, 180°	.46	.019
2		SMMS, forward flight	.49	.021

rearward flight with the AMMS skewed at $\beta = -30°$ (configurations 4 and 7) were found to be almost identical. This finding suggests that the fuselage orientation (forward versus rearward), as modeled, did not have a significant effect on the sight-wake and rotor-plane crossing point. In addition, the present study did not include the effects of engine inlet flow and exhaust, which could be important factors in determining the effect of fuselage orientation.

The sight shape and orientation did not have a significant effect on the mean-sight-wake and rotor-plane crossing location. However, the largest value of standard deviation in the sight-wake and rotor-plane crossing was noted for the configuration that yielded the highest vibration in flight (AMMS, sight skewed $\beta = -30°$ to the free stream, rearward flight at an advance ratio of 0.10). This finding indicates a higher level of unsteadiness in the sight wake for this configuration at this advance ratio.

The sight-wake shedding frequencies for configurations 2, 4, 6, 7, and 8 are shown in table 3. The mean vortex street shedding frequencies of the sights were approximately 60 Hz and 73 Hz at advance ratios of 0.07 and 0.10, respectively. The maximum difference in mean frequency for the various sights was approximately 24 percent at $\mu = 0.07$ and 17 percent at $\mu = 0.10$. The largest difference was noted for configurations 6 and 8 at the lower advance ratio (66 Hz versus 50 Hz), but this difference was not felt to contribute substantially to the adverse vibration observed in flight on the full-scale vehicle. For both advance ratios, the shed wake frequency was found to be the same for configurations 4 and 7, which suggests that the adverse vibration encountered in flight was not caused by the shed wake frequency exciting the rotor system. However, the strength of the shed vorticity, which cannot be measured visually, may differ for the various configurations. Methods to quantify the vorticity in the wake of the sight would be useful in documenting the differences between the wakes of the various sights.

Ideally, the wake shed from the sight should have the same Strouhal number for both the model and the full-scale tests. The Reynolds numbers of the model sights were estimated to be 280 000 and 420 000 for advance ratios of 0.07 and 0.10, respectively, based on free-stream airspeed. The Strouhal number is nonperiodic in this Reynolds number regime for circular and noncircular cylinders (refs. 15 and 16). This nonperiodicity correlates with the large standard deviation in the sight shedding frequencies shown in table 3. However, the Reynolds number for the full-scale vehicle is approximately four times greater than that for the model tests. At these higher Reynolds numbers, the Strouhal number for a circular cylinder starts to transition from nonperiodic to periodic (ref. 15). Therefore, the shed wake of the model mast-mounted sights should not be compared with the shed wake of the full-scale sights. A suggestion for making the shedding frequency characteristics of the model similar to those of the full-scale sight is to trip the model sight boundary layer.

Table 3. MMS-Wake Shedding Frequency

[Configuration numbers from fig.12]

Configuration	μ	Test condition	*f*, Hz	Std. dev.	*St*	Std. dev.	*Re*
7	0.07	AMMS, rearward flight, –30°	61	21	0.58	0.20	280 000
8		AMMS, rearward flight, 0°	50	10	.48	.10	
4		AMMS, forward flight, –30°	63	20	.60	.19	
6		AMMS, forward flight, 180°	66	20	.63	.19	
2		SMMS, forward flight	60	14	.54	.13	
7	0.10	AMMS, rearward flight, –30°	76	17	0.47	0.11	420 000
8		AMMS, rearward flight, 0°	76	20	.47	.12	
4		AMMS, forward flight, –30°	76	15	.47	.09	
6		AMMS, forward flight, 180°	72	19	.44	.11	
2		SMMS, forward flight	63	16	.37	.09	

Table 4. MMS Streamline Angle

[Configuration numbers from fig.12]

Configuration	μ	Test condition	Angle of attack, deg
7	0.07	AMMS, rearward flight, –30°	–22.4
8		AMMS, rearward flight, 0°	–20.8
4		AMMS, forward flight, –30°	–22.6
6		AMMS, forward flight, 180°	–19.0
2		SMMS, forward flight	–19.8
7	0.10	AMMS, rearward flight, –30°	–10.8
8		AMMS, rearward flight, 0°	–11.2
4		AMMS, forward flight, –30°	–11.4
6		AMMS, forward flight, 180°	–10.1
2		SMMS, forward flight	–10.6

Estimates of the sight streamline angle were made by measuring the angle of the smoke streamlines ahead of the leading edge of the sight with respect to the horizontal. Table 4 contains these results. For all configurations, the sights were observed to be operating at streamline angles of approximately –21° and –11° for advance ratios of 0.07 and 0.10, respectively. Negative angles indicate that the sights may have been lifting downward for these test conditions.

Lateral Light Sheet

A limited study utilizing the lateral light sheet was conducted at an advance ratio of 0.10 with only the

rearward fuselage shell. Configurations 3, 7, and 9 were investigated. In the following figures, the MMS and rotor blades (where visible) have been outlined for clarity.

Figures 18(a) to 18(c) show the lateral light sheet with an *r/R* of approximately 0.25 (19 in.) upstream of the rotor center for the three configurations. The camera was located downstream and to the left of the model. As shown in figure 18(a), the smoke was seen to exhibit a "mushroom" shape upstream of the AMMS with the AMMS skewed at $\beta = -30°$ to the free stream. This characteristic shape was not as pronounced upstream of the SMMS (fig. 18(c)), possibly because of differences in the placement of the smoke, which was higher than that for other configurations at this location for the SMMS.

As the light sheet was moved closer to the sight, some differences in the wake for the various configurations became apparent. Figures 19(a) to 19(c) show the smoke patterns with the light sheet positioned at the upstream edge of the sight. The smoke pattern for the SMMS (fig. 19(c)) and the AMMS skewed at $\beta = -30°$ to the free stream (fig. 19(a)) exhibited an increased curvature (relative to the smoke patterns of figs. 18(a) and 18(c)). The AMMS skewed at $\beta = 180°$ to the free stream (fig. 19(b)) does not exhibit this flow feature to the extent of the other cases, possibly because of the smaller radius of curvature of the leading edge of this configuration. Two nodes of recirculation were seen above the AMMS skewed at $\beta = -30°$ to the free stream (fig. 19(a)). The nodes of recirculation were noted to pulse significantly in the vertical plane.

Flow characteristics with the light sheet positioned on the center of the sight are shown in figure 20. The AMMS skewed $\beta = -30°$ to the free stream (fig. 20(a)) exhibited the two nodes of recirculation above the sight surface. The vertical pulsing of the nodes of recirculation was diminished relative to figure 19(a). These flow features were not evident in the other configurations shown in figures 20(b) and 20(c).

More detail of the wake structure of the AMMS skewed $\beta = -30°$ to the free stream was seen with the light sheet positioned on the downstream edge of the sight, as shown in figure 21(a). Analysis of the video data showed asymmetrical vortex structures that were observed to rotate in a manner that produces negative or downward lift and was consistent with the observation of negative angle of attack at the sights noted previously. However, results from a wind tunnel test conducted at the Texas A&M Low Speed Wind Tunnel[1] in December 1991 on a 50-percent scale sight alone showed that the sight produced slightly positive lift at angles of attack greater than −25°. This positive lift found in the Texas A&M wind tunnel test was attributed to the pedestal unit and the slight camber of the AMMS. The investigation was unable to include the highly complex rotor wake, which may explain the apparent negative lift produced by the AMMS found in the present investigation. Measurements obtained with laser velocimetry on a helicopter model without a mast-mounted sight have shown that the inflow near the center of the rotor has substantial velocity gradients (ref. 17). Also shown in figure 21(a), on the retreating side of the AMMS, was a secondary vortex that was noted to rotate in the opposite sense as the primary vortex. No clearly definable flow patterns were noted for the other configurations (figs. 21(b) and 21(c)).

Figure 22 contains flow characteristics at a point $r/R = 0.25$ downstream of the sights. Configuration 7 clearly exhibited a wake with a well-defined pattern, as shown in figure 22(a). The nodes of recirculation, shown in figures 19(a), 20(a), and 21(a), are no longer present in figure 22(a). The active and well-defined wake of the AMMS skewed $\beta = -30°$ to the free stream is in marked contrast to the other two configurations tested (figs. 22(b) and 22(c)) that did not have a clearly defined wake pattern. These test results are in qualitative agreement with the Texas A&M wind tunnel tests that were sponsored by Martin Marietta Corporation on the AMMS alone and conducted after the present investigation. Martin Marietta also performed a velocity survey behind the sight with a seven-hole pressure probe. In this survey, the AMMS skewed $\beta = -30°$ to the free stream was reported to have elevated levels of vorticity (calculated using the velocity survey data) as compared with the other configurations (SMMS and AMMS skewed $\beta = -90°$, $-60°$, and $0°$). Martin Marietta also reported the results of a limited laser light sheet flow visualization investigation that verified that the AMMS had a more active and defined wake than the SMMS.

Figure 23 is a sketch of the wake structure and rotation, at various light sheet locations and based on video analysis, for the AMMS skewed $\beta = -30°$ to the free stream. Flow structures that may have existed directly beneath the sight were not visible for stations 2 and 3 because of optical blockage of the light sheet by the AMMS.

Figure 24 shows the flow field structure obtained with the light sheet located where the sight wakes crossed the rotor plane. The MMS were not visible in these figures. The rotor blades have been outlined for clarity. For configuration 7, the vortices trailed from the sight were still visible (fig. 24(a)). The wakes from the other configurations, however, were devoid of any

[1]Wind tunnel test results published in Martin Marietta Corporation report number TRP-80850680-004.

coherent structure (figs. 24(b) and 24(c)). The appearance of vortices near the rotor plane for configuration 7 could be significant because of similarity to blade tip vortices known to cause sharp and rapid changes in blade loads and thus cause adverse vibration (ref. 18).

The wake of the AMMS skewed $\beta = -30°$ to the free stream was examined after it passed under the rotor plane to determine whether the rotor dissipated these trailed vortices. Figure 25 shows that significant vortex structure still existed under the rotor. Although not shown, no vortex structure was discernible in the video data from the other two configurations tested. The significant vortex structure, which passed through the rotor system, was noticed to pass close to the nose of the model (fig. 26) and could be a possible contributor to the adverse vibration problem through fuselage excitation. However, because the forward flight fuselage (configuration 4) was not tested with a lateral light sheet, differences in the sight wake for configurations 4 and 7 cannot be qualified. Also, additional instrumentation in the forward fuselage area, such as pressure transducers, would have been useful in defining unsteady aerodynamics in this area.

Concluding Remarks

An exploratory flow visualization investigation was conducted with a laser light sheet system on a 27-percent-scale AH-64 attack helicopter model fitted with various mast-mounted-sight (MMS) configurations in the Langley 14- by 22-Foot Subsonic Tunnel. The investigation was conducted to identify aerodynamic phenomena that may have contributed to adverse vibration encountered during full-scale flight testing of an Apache/Longbow configuration. Several aerodynamic characteristics of MMS in the presence of a rotor and fuselage were identified that may lead to an eventual understanding of the vibration problem.

Analysis of lateral light sheet plane data implies significant vortex structure in the wake of the asymmetric mast-mounted sight (AMMS) skewed −30° to the free stream (configuration with maximum in flight vibration) that was absent from the AMMS skewed at 180° to the free stream and the symmetric mast-mounted sight (SMMS) (configurations with no increased adverse vibration in flight). The AMMS skewed −30° to the free stream had a wake that was more defined than the SMMS wake. Trailed vortices were indicated from both edges of the AMMS skewed −30° to the free stream. This wake pattern remained discernible after passing through the rotor system and was in close proximity to the nose of the model.

Analysis of longitudinal light sheet plane data, with the light sheet placed on the center of the sight for all configurations, indicated a nonperiodic coherent vortex shed from the sights. Analysis of the video data quantified the frequency of the shed wake and the location of the wake and rotor-plane crossing. The mean-sight-wake and rotor-plane crossing points were estimated to be $\bar{r}/R = 0.37$ and 0.46 for advance ratios of 0.07 and 0.10, respectively. The mean vortex street shedding frequencies of the sights were approximately 60 and 73 Hz at advance ratios of 0.07 and 0.10, respectively. Large standard deviation, on the order of 10 to 20 Hz, was noted for the shedding frequency of the sights. No significant effects from the sight-wake and rotor-plane crossing location or the sight-wake frequency results were noted as a possible source of the adverse vibration. The MMS streamline angles were approximately −21° and −11° for advanced ratios of 0.07 and 0.10, respectively.

NASA Langley Research Center
Hampton, VA 23681-0001
January 24, 1995

References

1. Gentry, Garl L., Jr.; Quinto, P. Frank; Gatlin, Gregory M.; and Applin, Zachary T.: *The Langley 14- by 22-Foot Subsonic Tunnel: Description, Flow Characteristics, and Guide for Users*. NASA TP-3008, 1990.

2. Murrill, Robert J.: *Operation and Maintenance Manual for the General Rotor Model System*. NASA CR-145230, 1977.

3. Heyson, H. H.: *Use of Superposition in Digital Computers To Obtain Wind Tunnel Interference Factors for Arbitrary Configurations, With Particular Reference to V/STOL Models.* NASA TR R-302, 1969.

4. Leighty, Bradley D.; Rhodes, David B.; Franke, John M.; and Jones, Stephen B.: *A Synchronous Strobed Laser Light Sheet for Rotor Flow Visualization*. NASA TM-4266, 1991.

5. Ghee, Terence A.; and Elliott, Joe W.: A Study of the Rotor Wake of a Small-Scale Rotor Model in Forward Flight Using Laser Light Sheet Flow Visualization With Comparisons to Analytical Models. *Proceedings of the 48th Annual Forum*, Volume 1, American Helicopter Soc., 1992, pp. 697–719.

6. Wilson, John C.: A General Rotor Model System for Wind-Tunnel Investigations. *J. Aircr.*, vol. 14, no. 7, July 1977, pp. 639–643.

7. Straub, F. K.; Johnston, R. A.; Head, R. E.; and Kelley, H. L.: Design and Development of a Dynamically Scaled Model AH-64 Main Rotor. *Vertica*, vol. 9, no. 2, 1985, pp. 165–180.

8. Kelley, Henry L.: *Effect of Planform Taper on Hover Performance of an Advanced AH-64 Model Rotor.* NASA TM-89145, AVSCOM TM-87-B-10, 1987.

9. Bingham, Gene J.; and Noonan, Kevin W.: *Two-Dimensional Aerodynamic Characteristics of Three Rotorcraft Airfoils at*

Mach Numbers From 0.35 to 0.90. NASA TP-2000, AVRAD-COM TR 82-B-2, 1982.

10. Picasso, Bartholomew D., III; Downs, Gary T.; Buckanin, Robert M.; and Herbst, Michael K.: *Airworthiness and Flight Characteristics (A&FC) Test of YAH-64 Advanced Attack Helicopter, Prototype Qualification Test-Government (PQT-G), Part 3 and Production Validation Test-Government (PVT-G) for Handbook Verification*. USAAEFA Proj. No. 80-17-3, U.S. Army, Oct. 1982. (Available from DTIC as AD A130 524.)

11. Kudlinski, Robert A.; and Park, Stephen K.: *Digital Enhancement of Flow Field Images*. NASA TP-2770, 1988.

12. Lamar, John E.; and Johnson, Thomas D.: *Sensitivity of F-106B Leading-Edge-Vortex Images to Flight and Vapor-Screen Parameters*. NASA TP-2818, 1988.

13. Ahmed, A.; Khan, M. J.; and Bays-Muchmore, B.: Experimental Investigation of a Three-Dimensional Bluff Body Wake. AIAA-92-0429, Jan. 1992.

14. The Japan Society of Mechanical Engineers, eds.: *Visualized Flow—Fluid Motion in Basic and Engineering Situations Revealed by Flow Visualization*. Pergamon Press, 1988.

15. Schlichting, Hermann (J. Kestin, transl.): *Boundary-Layer Theory*, Seventh ed., McGraw-Hill Book Co., 1979.

16. Delany, Noel K.; and Sorensen, Norman E.: *Low-Speed Drag of Cylinders of Various Shapes*. NACA TN-3038, 1953.

17. Elliott, Joe W.; Althoff, Susan L.; and Sailey, Richard H.: *Inflow Measurement Made With a Laser Velocimeter on a Helicopter Model in Forward Flight. Volume 1—Rectangular Planform Blades at an Advance Ratio of 0.15*. NASA TM-100541, AVSCOM TM-88-B-004, 1988.

18. Lorber, P. F.: Blade-Vortex Interaction Data Obtained From a Pressure-Instrumented Model UH-60A Rotor at the DNW. *J. American Helicopter Soc.*, vol. 38, no. 3, July 1993, pp. 26–34.

Figure 1. AH-64D Apache Longbow attack helicopter with asymmetric sight installed.

Figure 2. Model of asymmetric sight, 27-percent scale.

Figure 3. Model of symmetric sight, 27-percent scale.

(a) Aerial view.

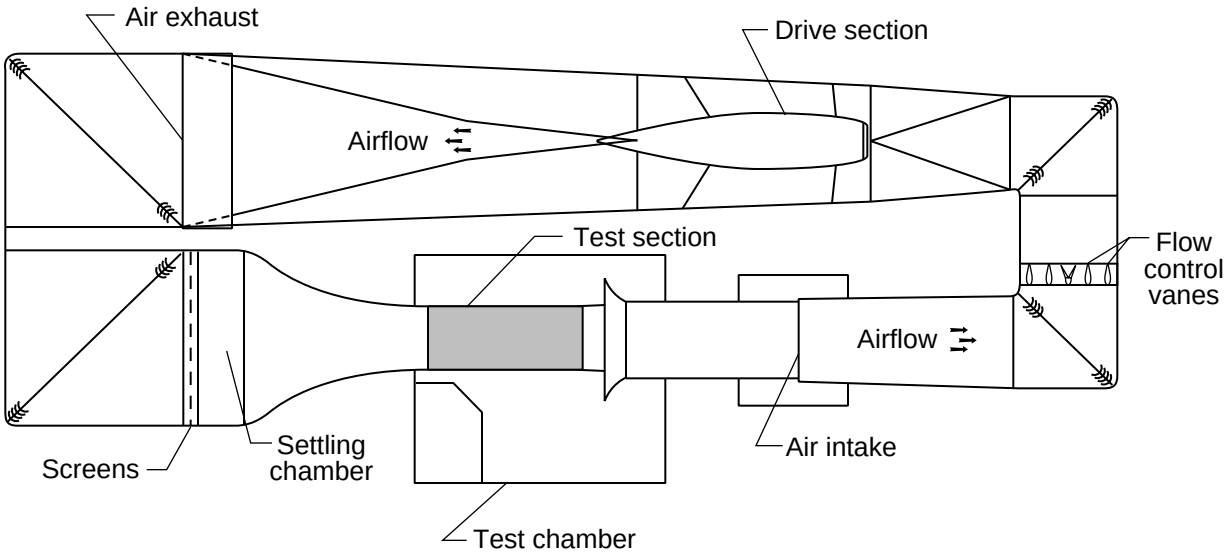

(b) Schematic.

Figure 4. Langley 14- by 22-Foot Subsonic Tunnel.

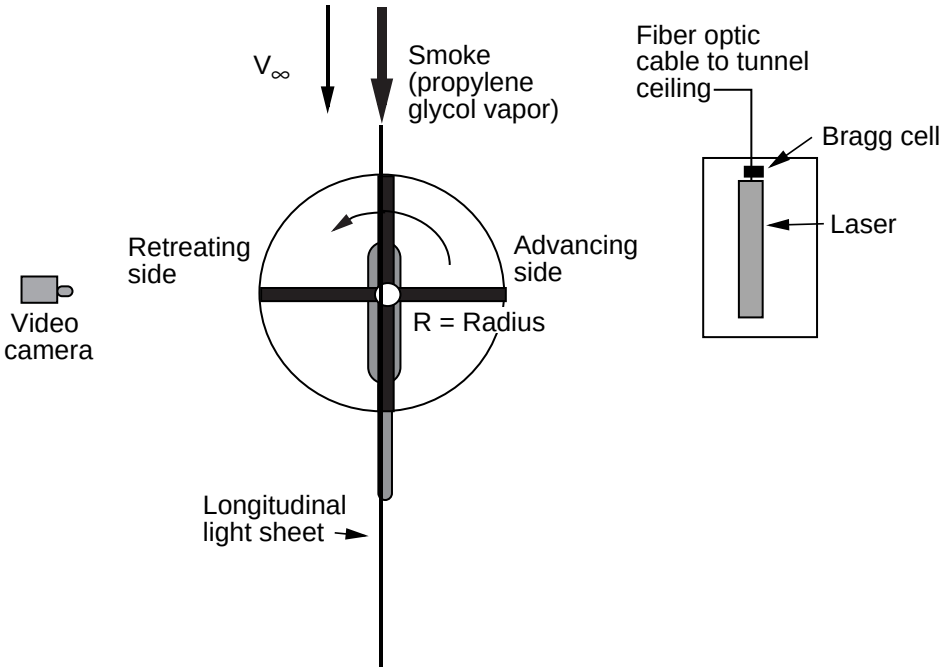

Figure 5. Schematic of experimental setup.

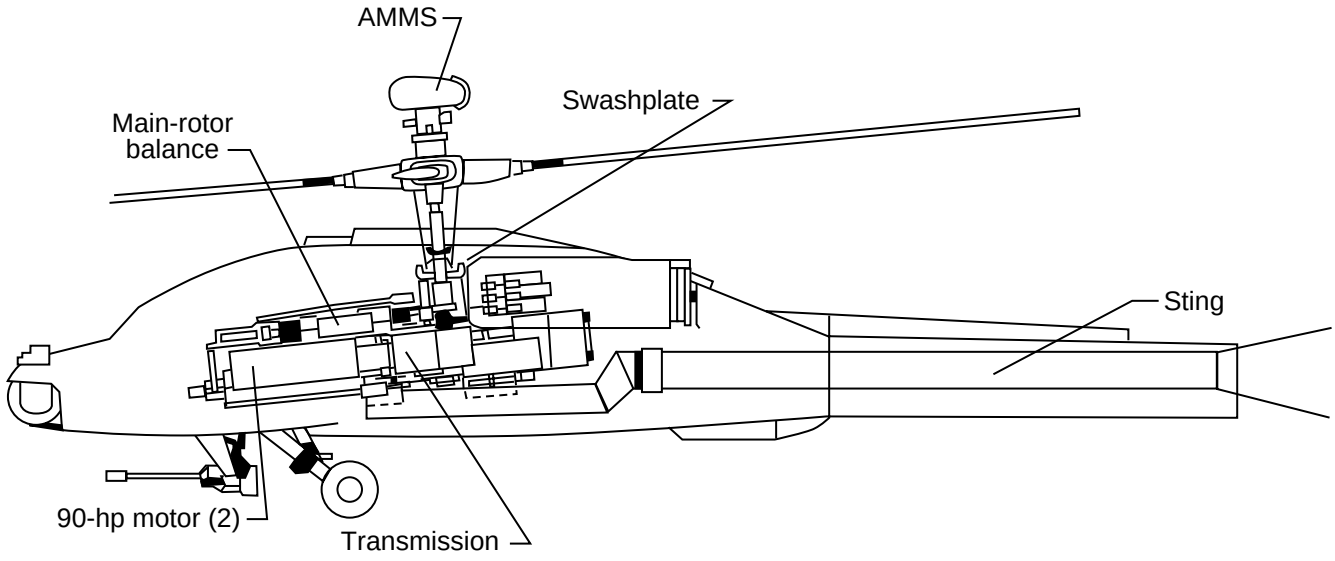

Figure 6. AH-64 fuselage model (forward flight configuration) with AMMS installed on General Rotor Model System.

Advanced Rotor (3:1 Taper)

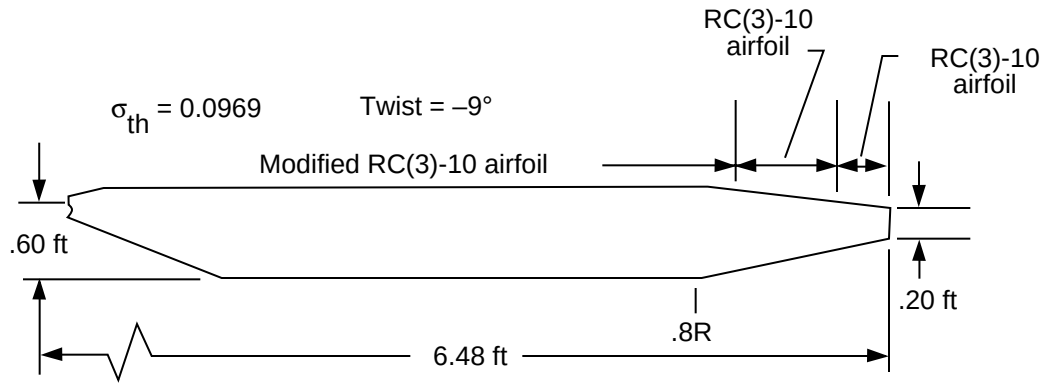

Baseline Rotor

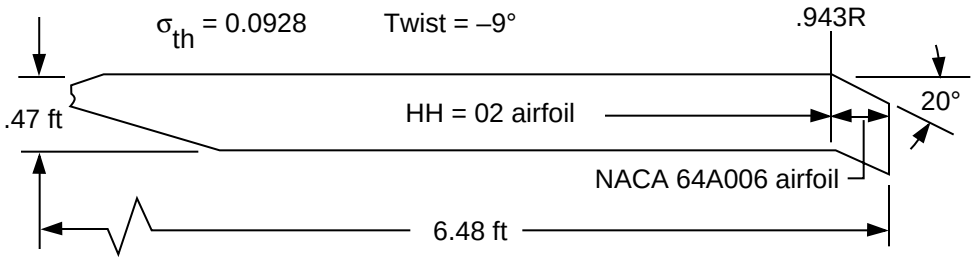

Figure 7. Geometric characteristics of rotor blade.

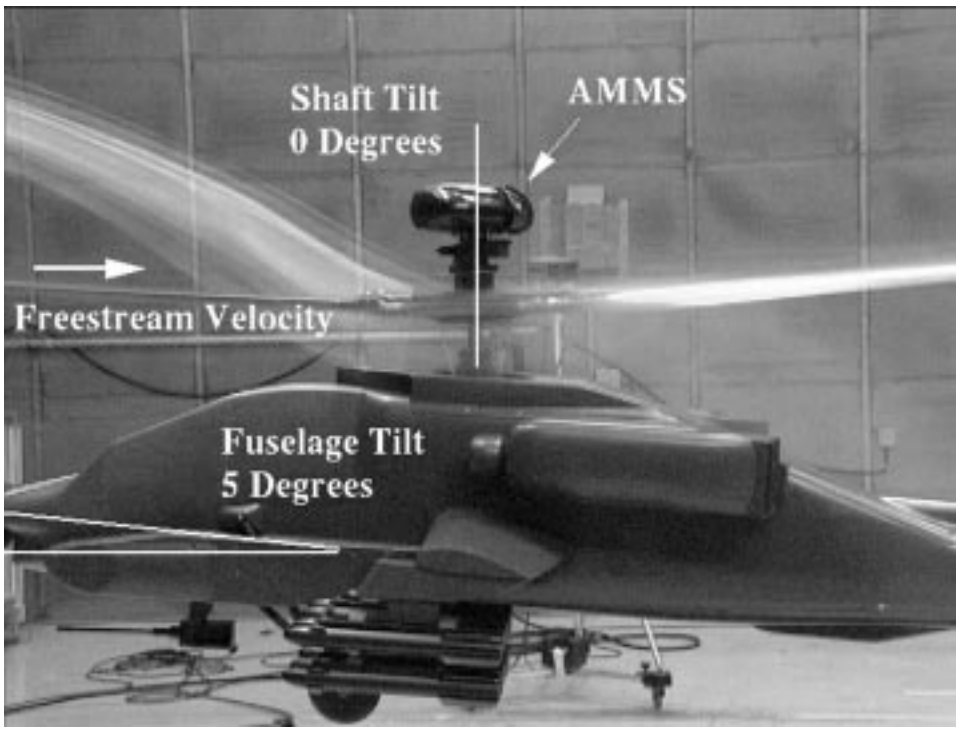

Figure 8. Fuselage shell used in forward flight portion of investigation.

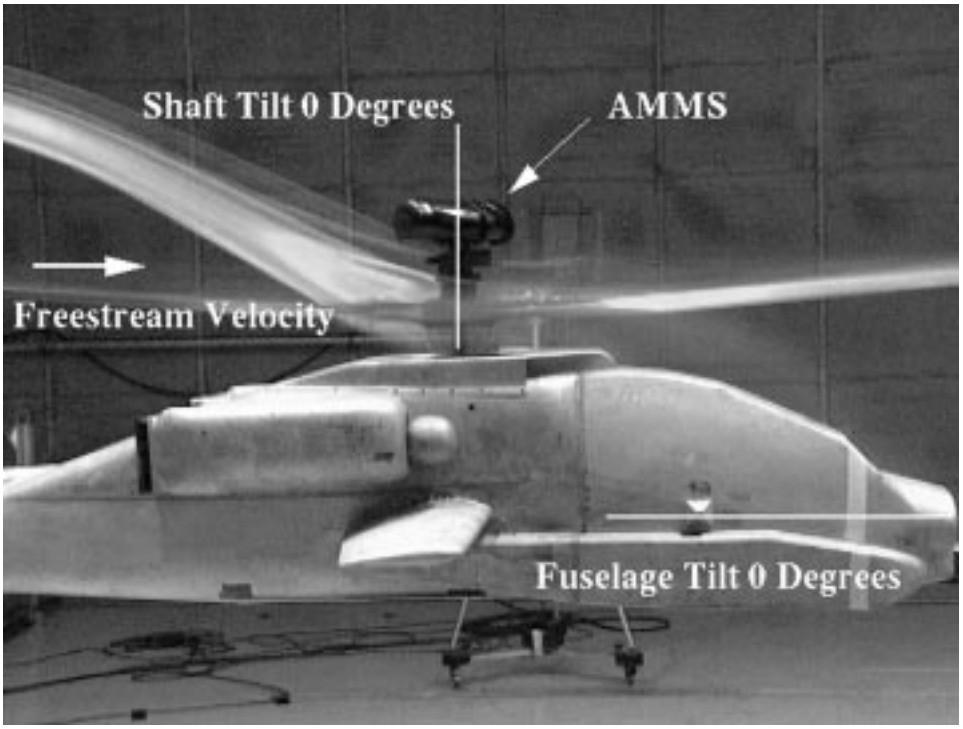

Figure 9. Fuselage shell used in rearward flight portion of investigation.

Figure 10. Overhead view of model sights and pedestal.

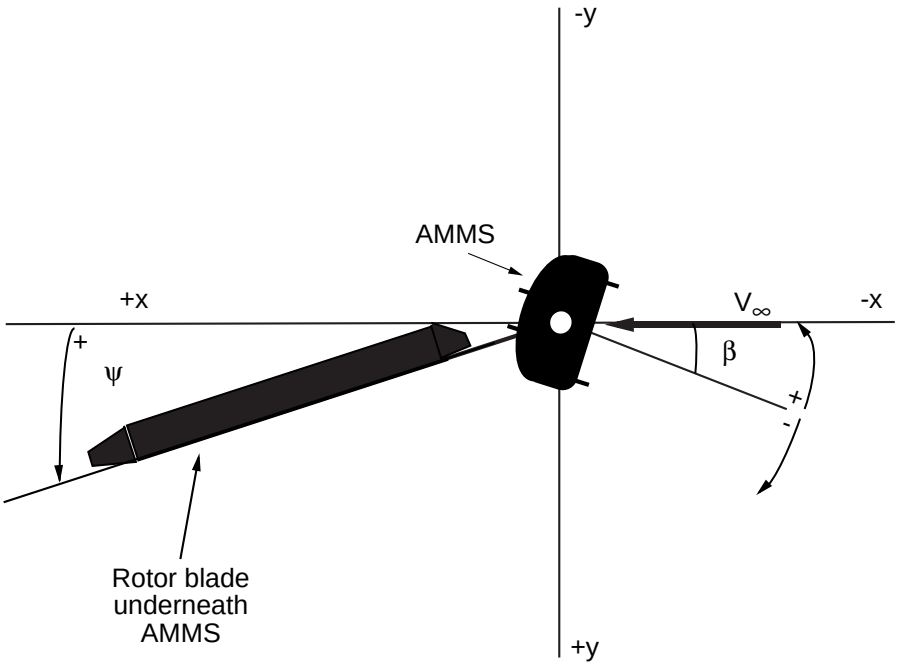

Figure 11. Sign convention of AMMS skew angle and rotor system.

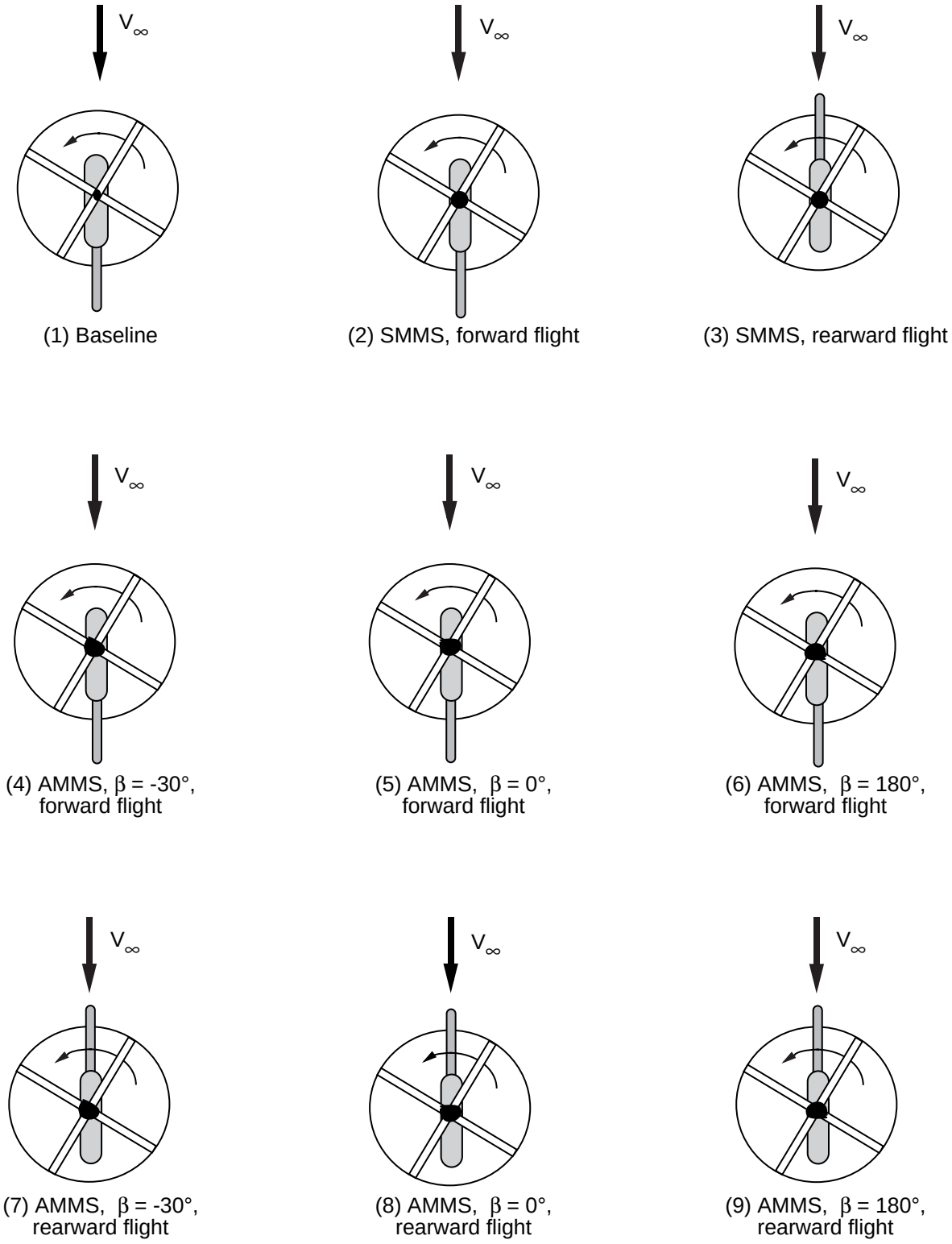

Figure 12. Schematics of configurations tested.

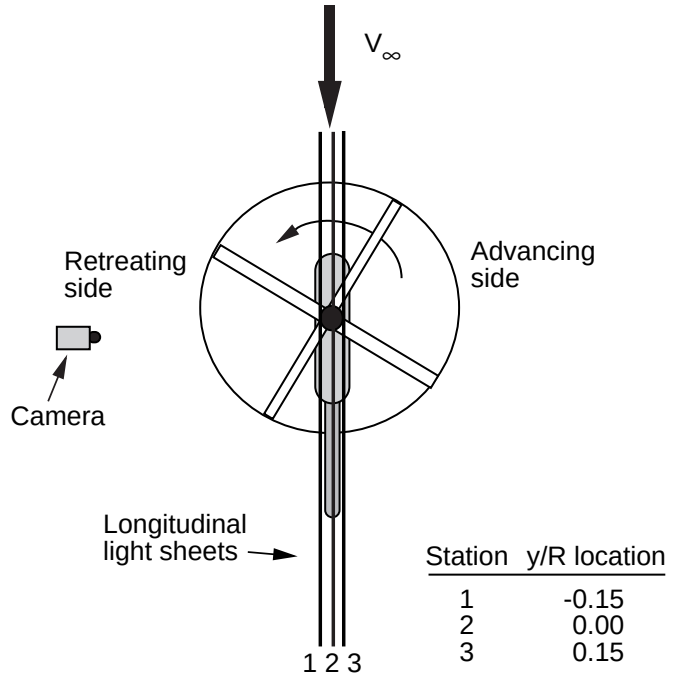

Figure 13. Testing locations of longitudinal laser light sheets.

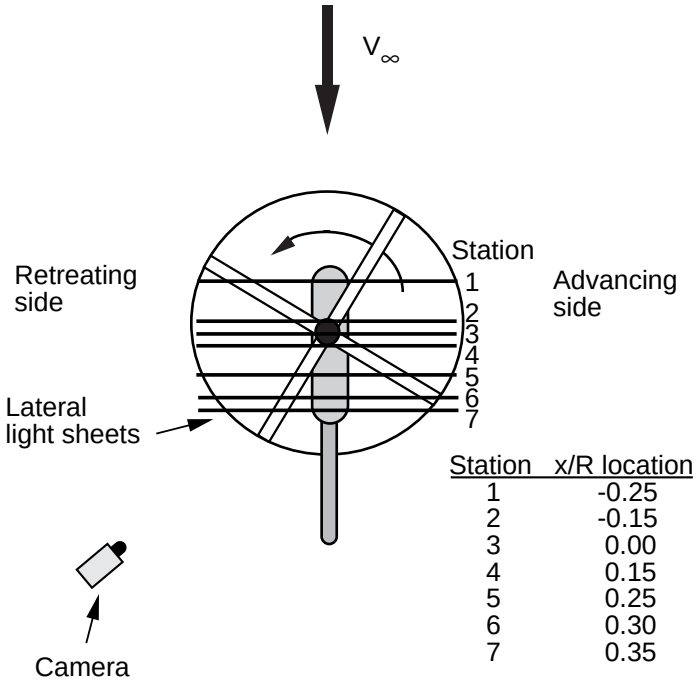

Figure 14. Testing locations of lateral laser light sheets.

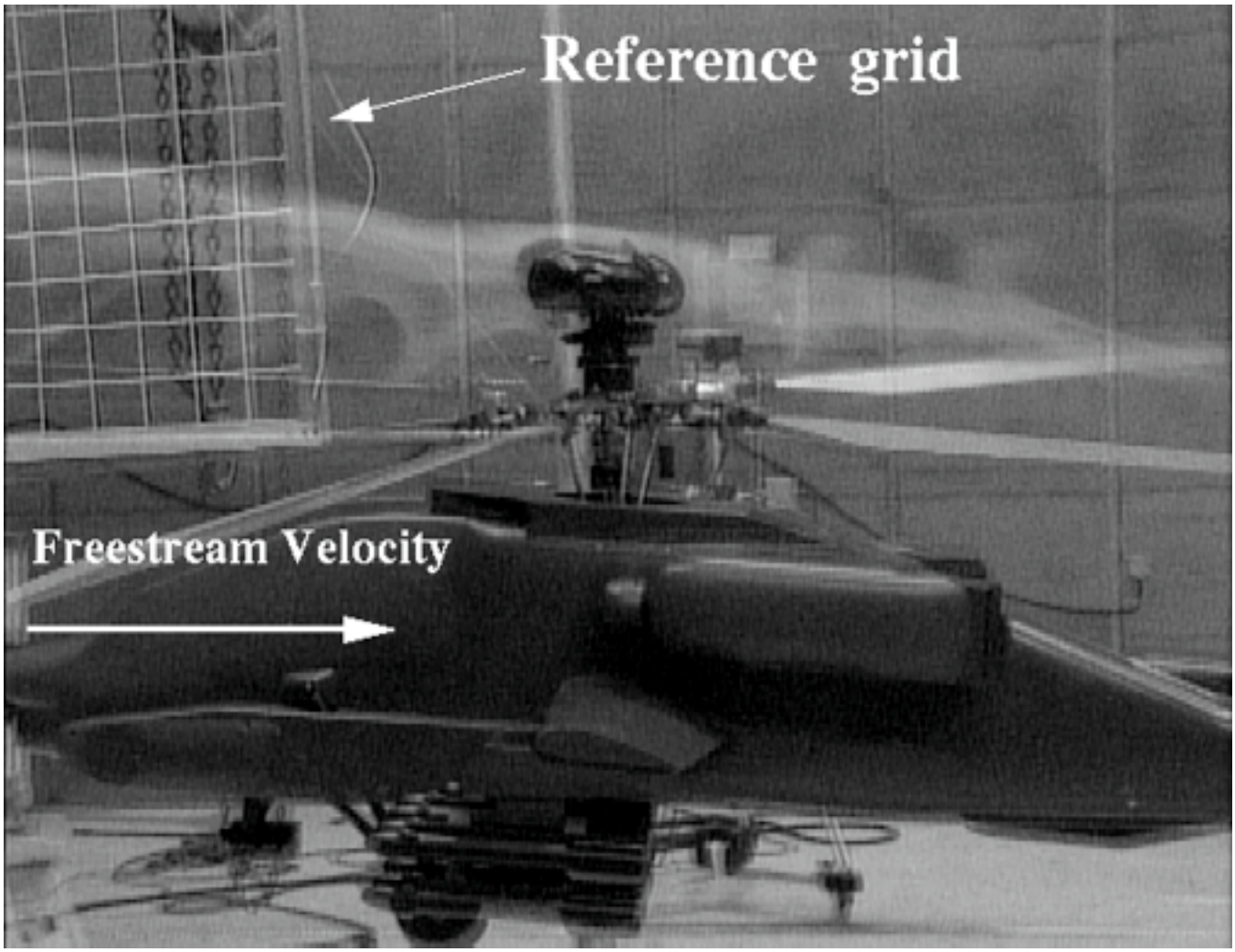

Figure 15. Superposition of reference grid image on video image.

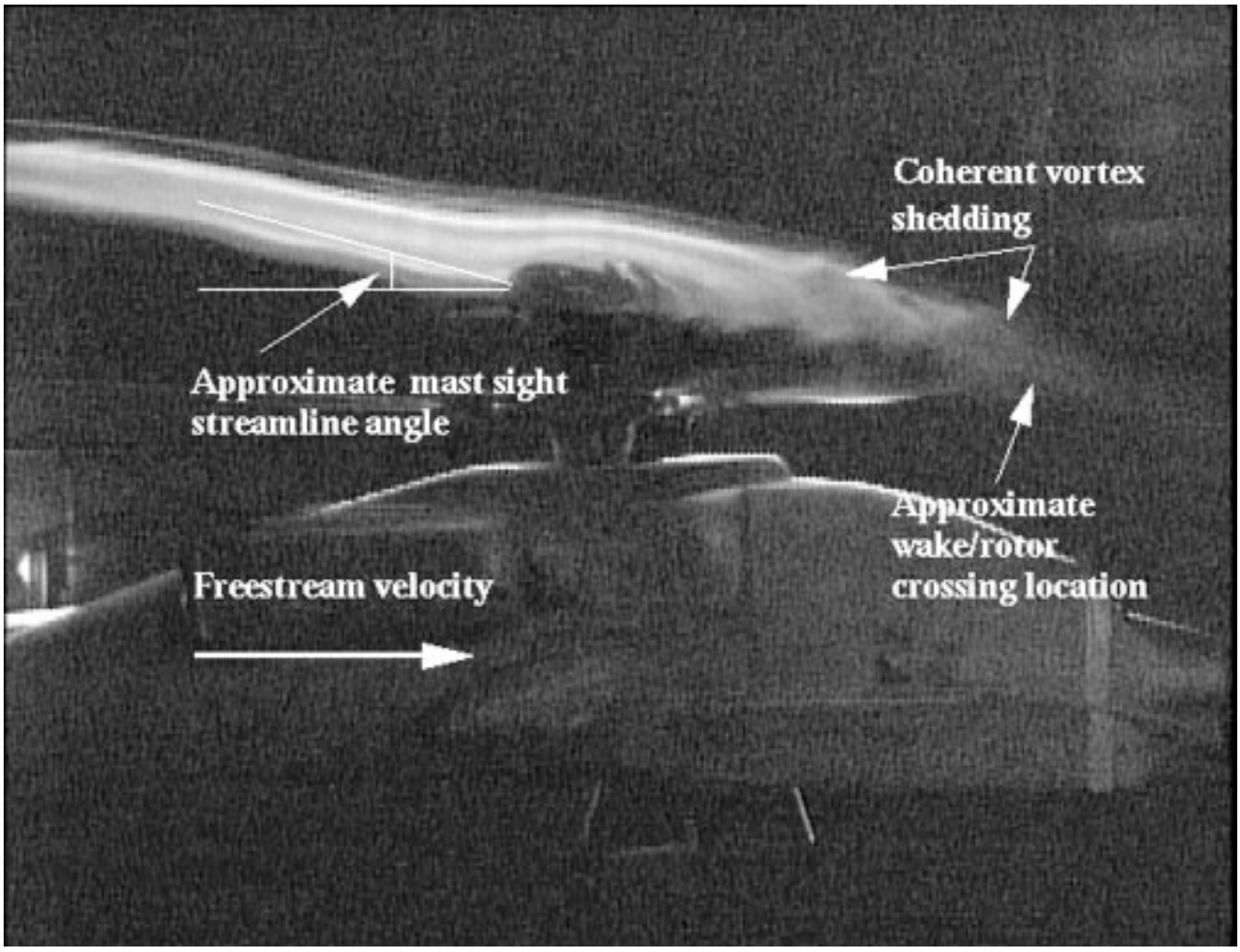

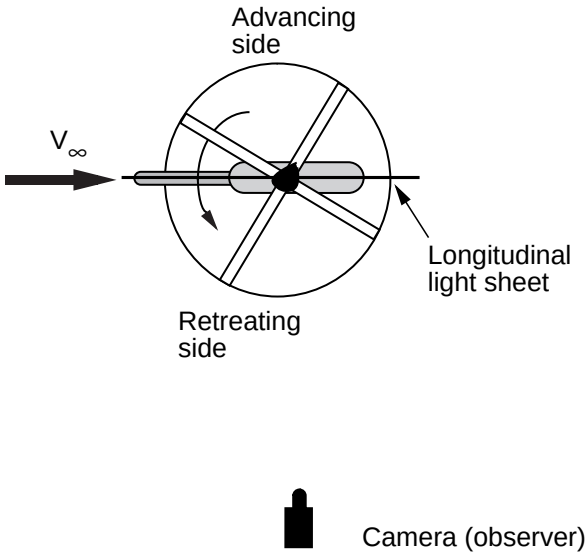

Figure 16. Typical longitudinal light sheet video image with annotations of flow features for the AMMS. $\mu = 0.10$; rearward flight; configuration 7.

Figure 17. Baseline configuration in forward flight, with $\mu = 0.07$.

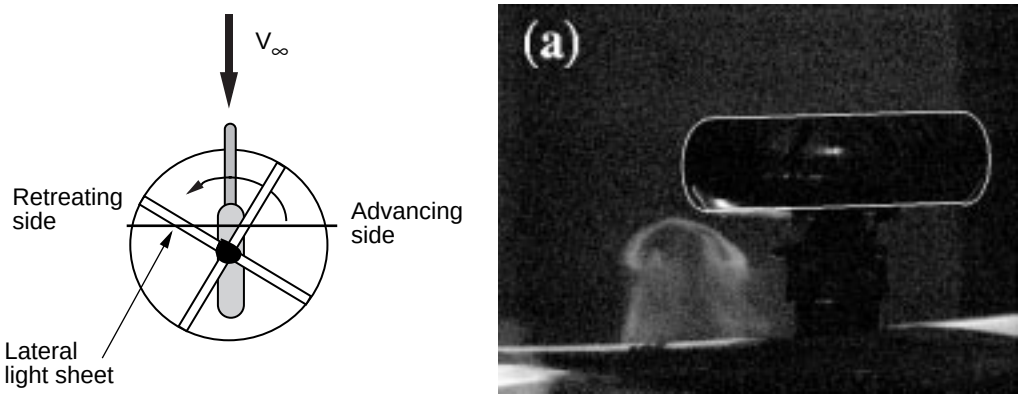

(a) AMMS skewed at −30°.

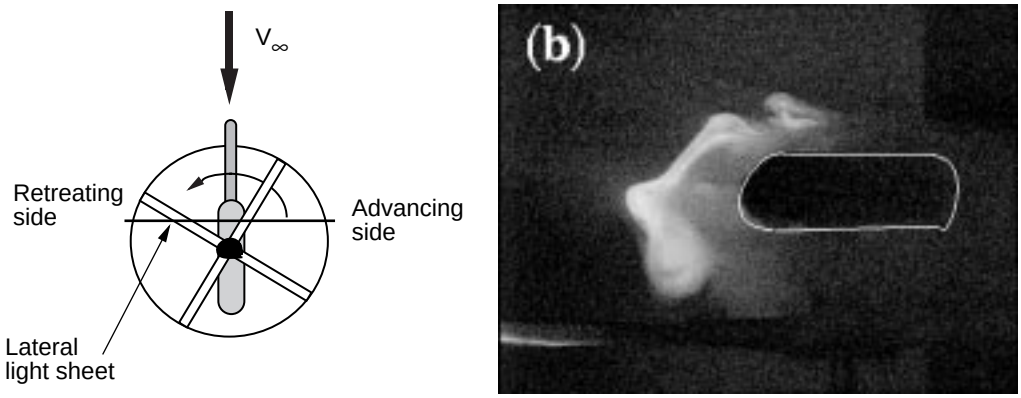

(b) AMMS skewed at 180°.

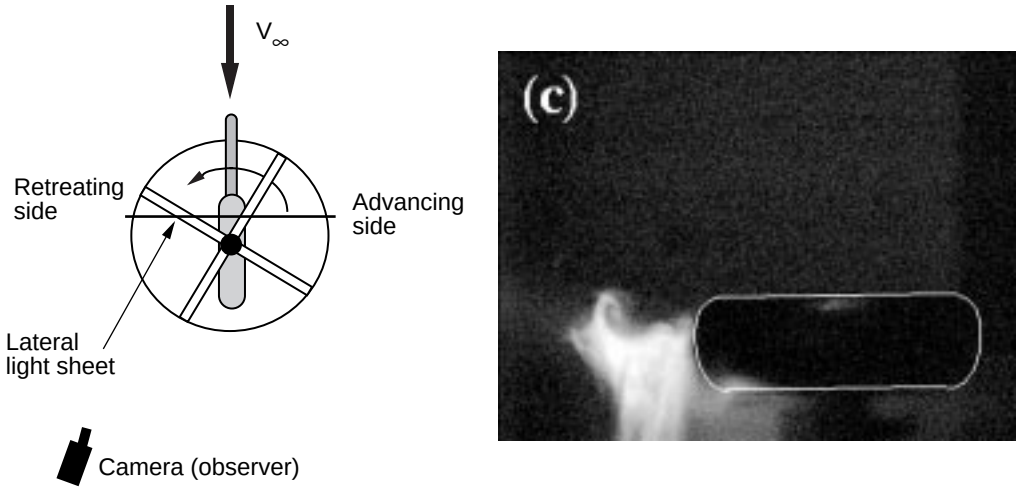

(c) SMMS.

Figure 18. Lateral light sheet video images for station 1, r/R = 0.25 upstream of hub, with μ = 0.10.

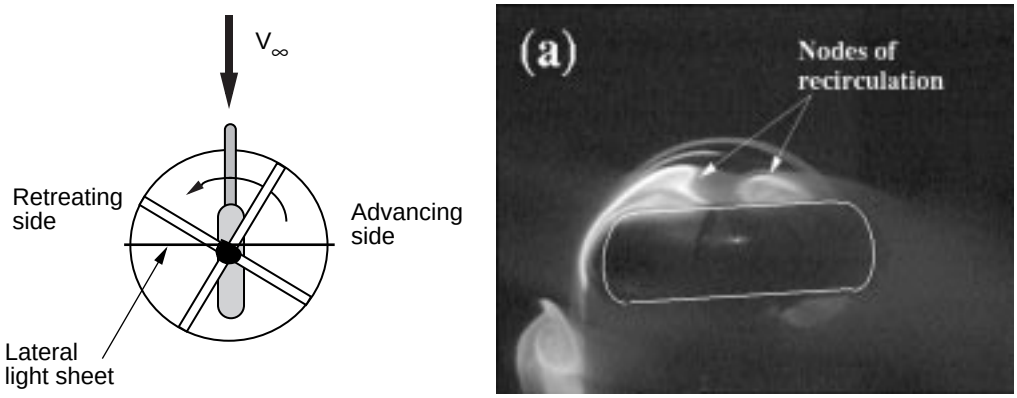

(a) AMMS skewed at −30°.

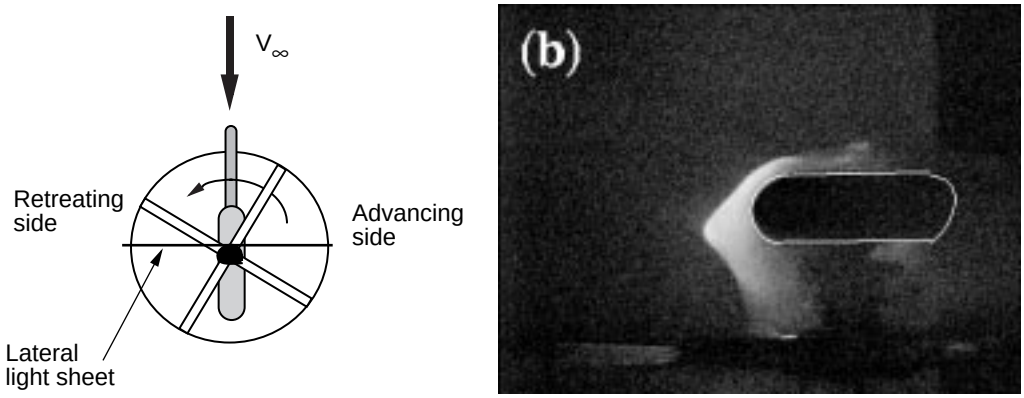

(b) AMMS skewed at 180°.

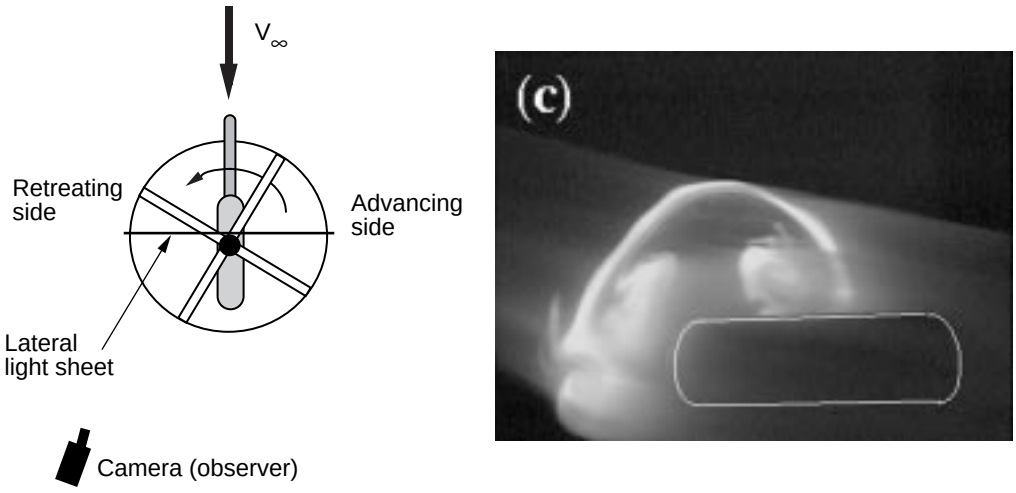

(c) SMMS.

Figure 19. Lateral light sheet video images for station 2, leading edge of sight, with $\mu = 0.10$.

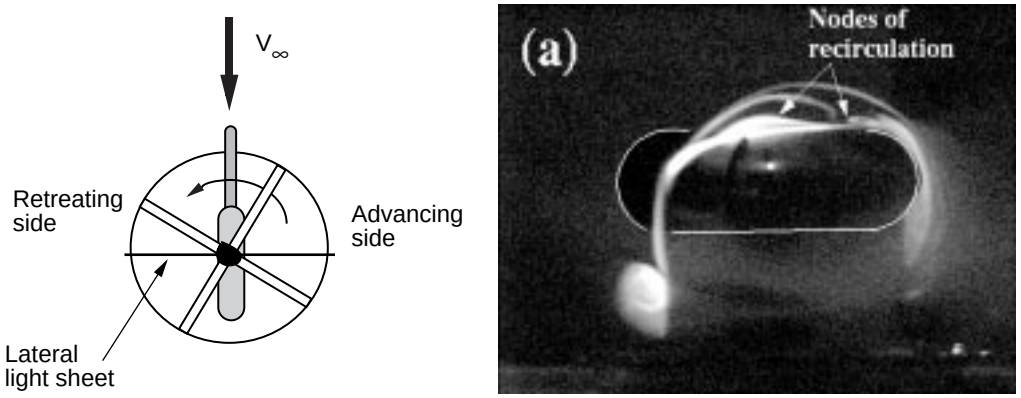

(a) AMMS skewed at –30°.

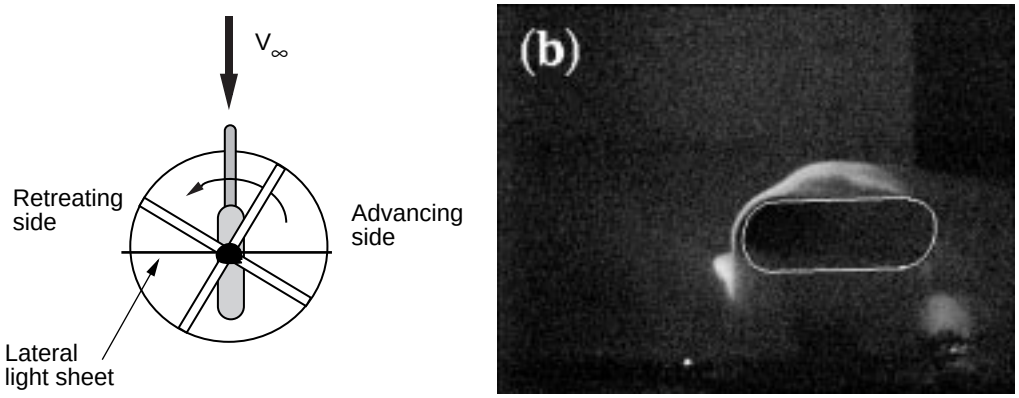

(b) AMMS skewed at 180°.

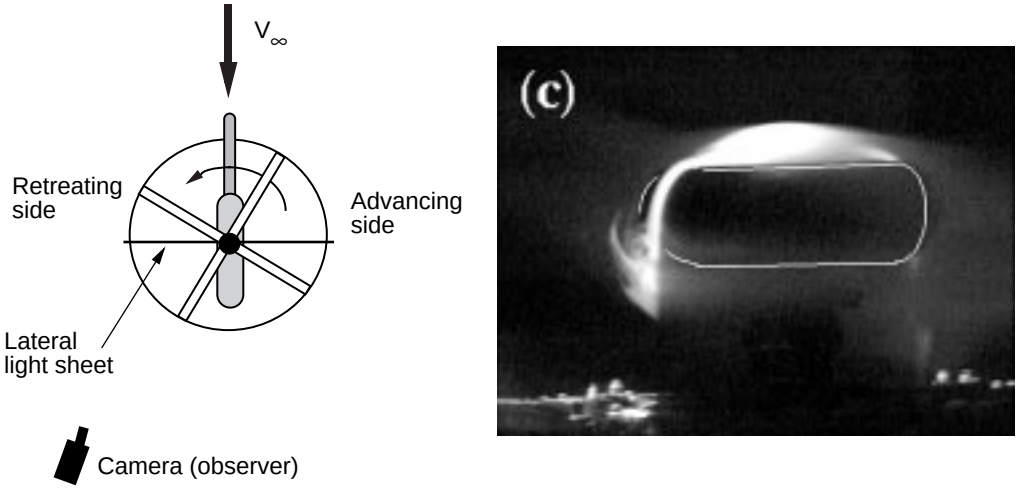

(c) SMMS.

Figure 20. Lateral light sheet video images for station 3, center of sight, with $\mu = 0.10$.

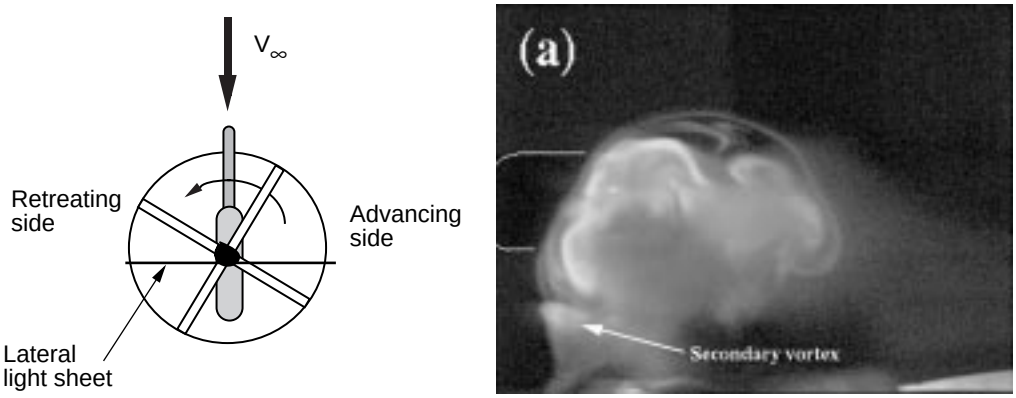

(a) AMMS skewed at –30°.

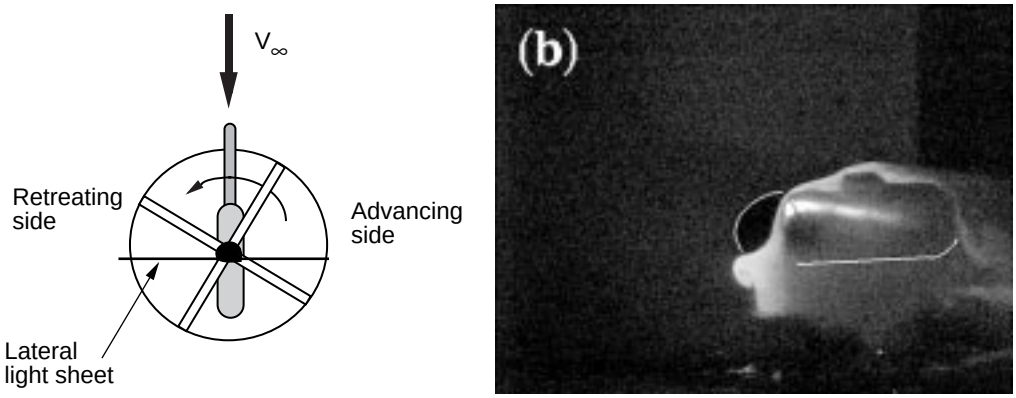

(b) AMMS skewed 180°.

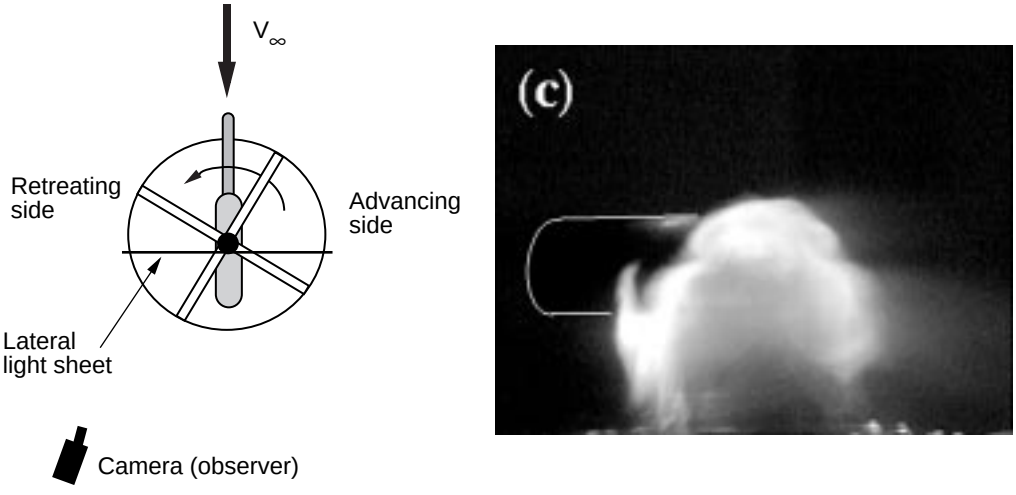

(c) SMMS.

Figure 21. Lateral light sheet video images for station 4, trailing edge of sight, with $\mu = 0.10$.

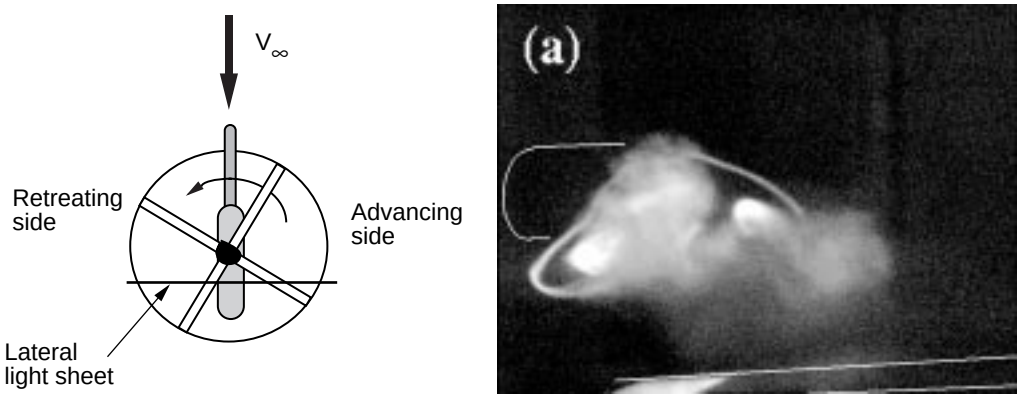

(a) AMMS skewed at −30°.

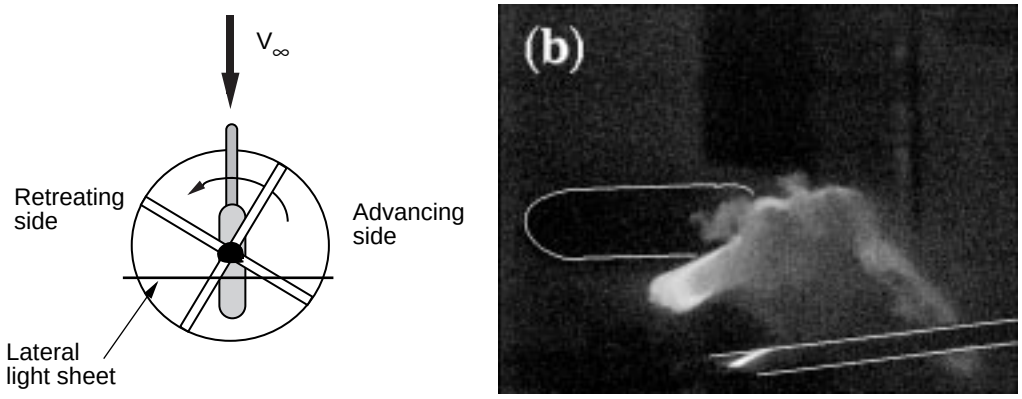

(b) AMMS skewed at 180°.

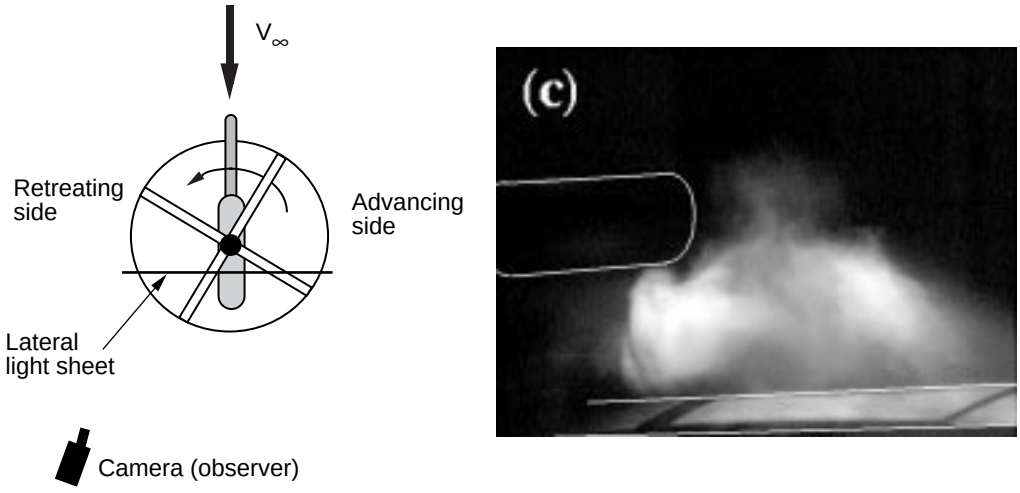

(c) SMMS.

Figure 22. Lateral light sheet video images for station 5, r/R = 0.25 downstream of hub, with μ = 0.10.

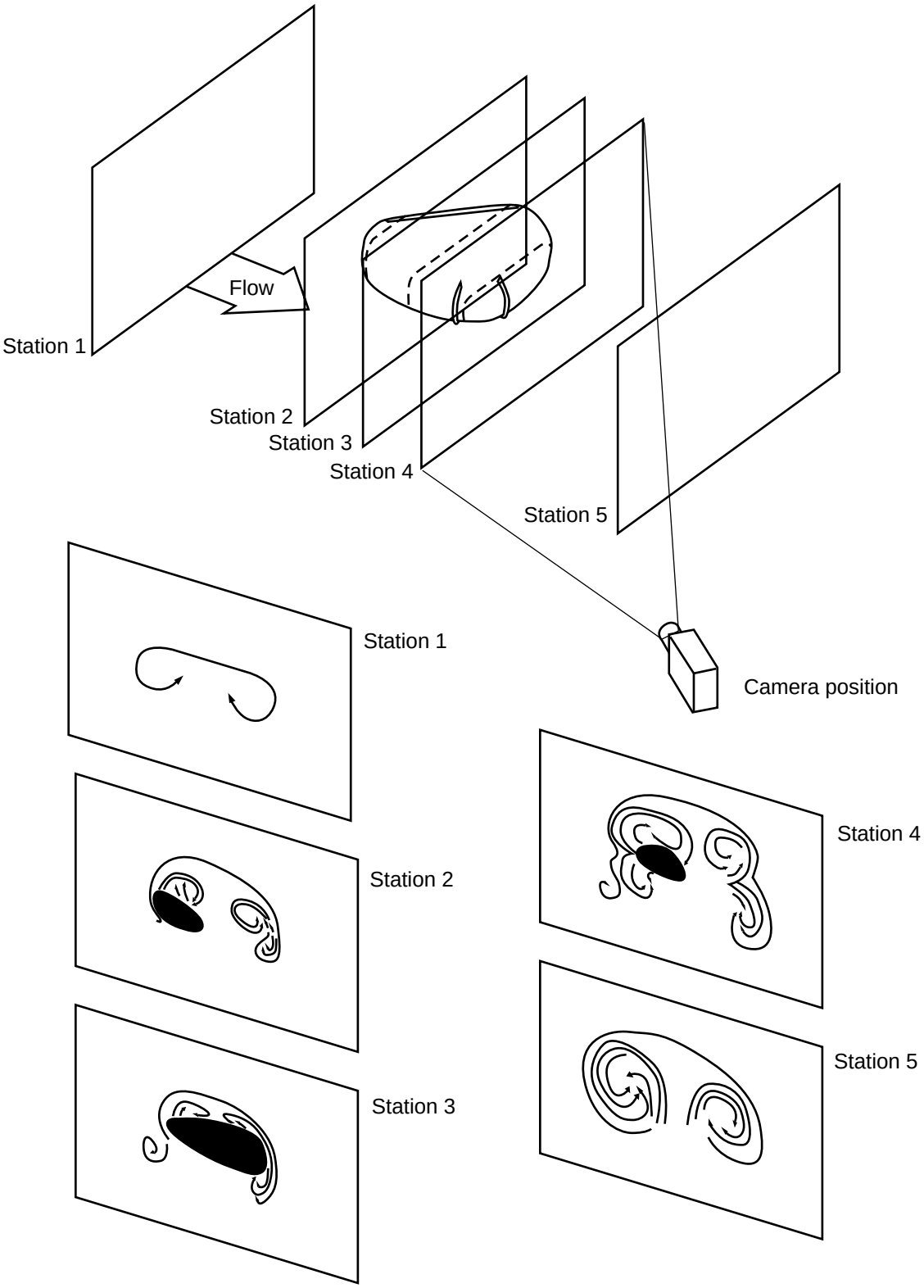

Figure 23. Sketch of wake, based on video analysis, of AMMS skewed –30° to free stream.

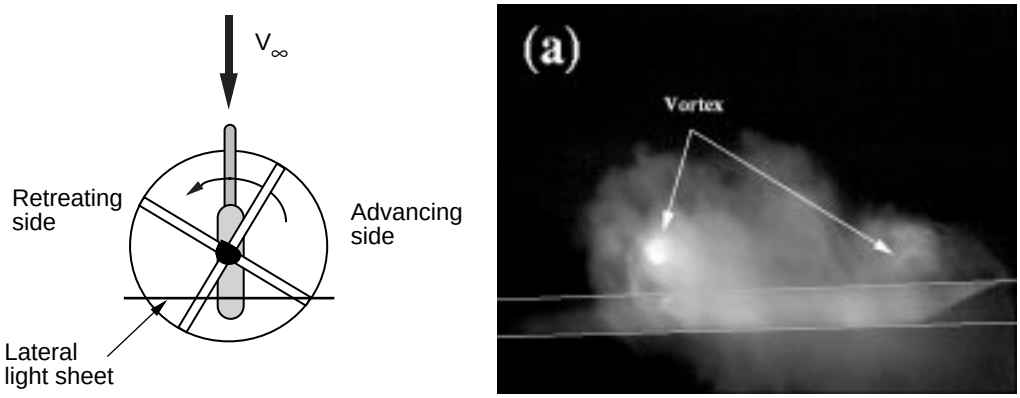

(a) AMMS skewed at −30°.

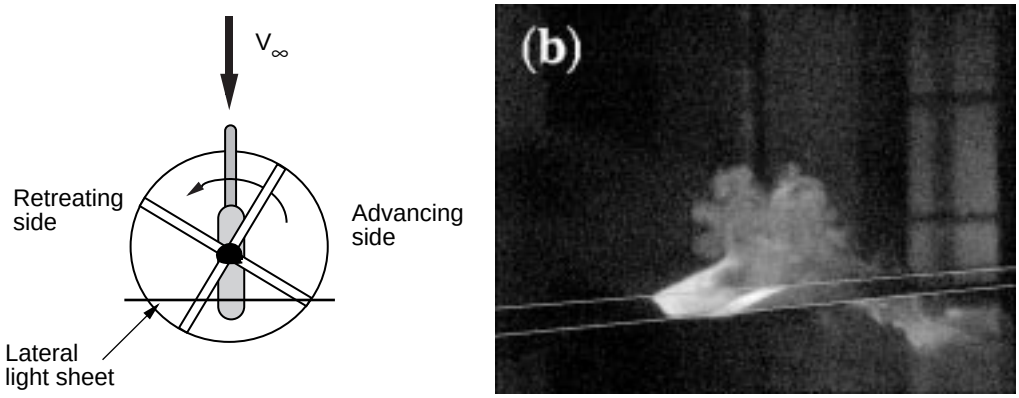

(b) AMMS skewed at 180°.

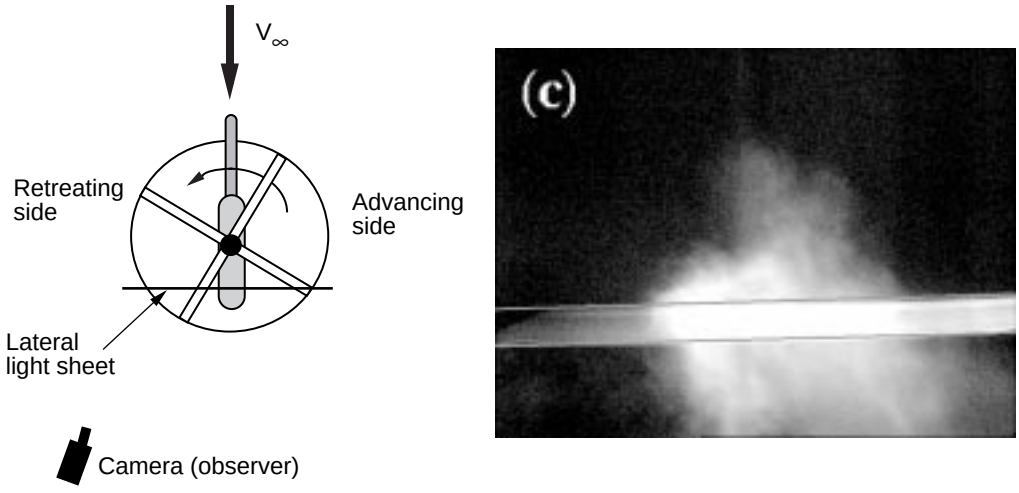

(c) SMMS.

Figure 24. Lateral light sheet video images for station 6, rotor plane crossing point, with $\mu = 0.10$.

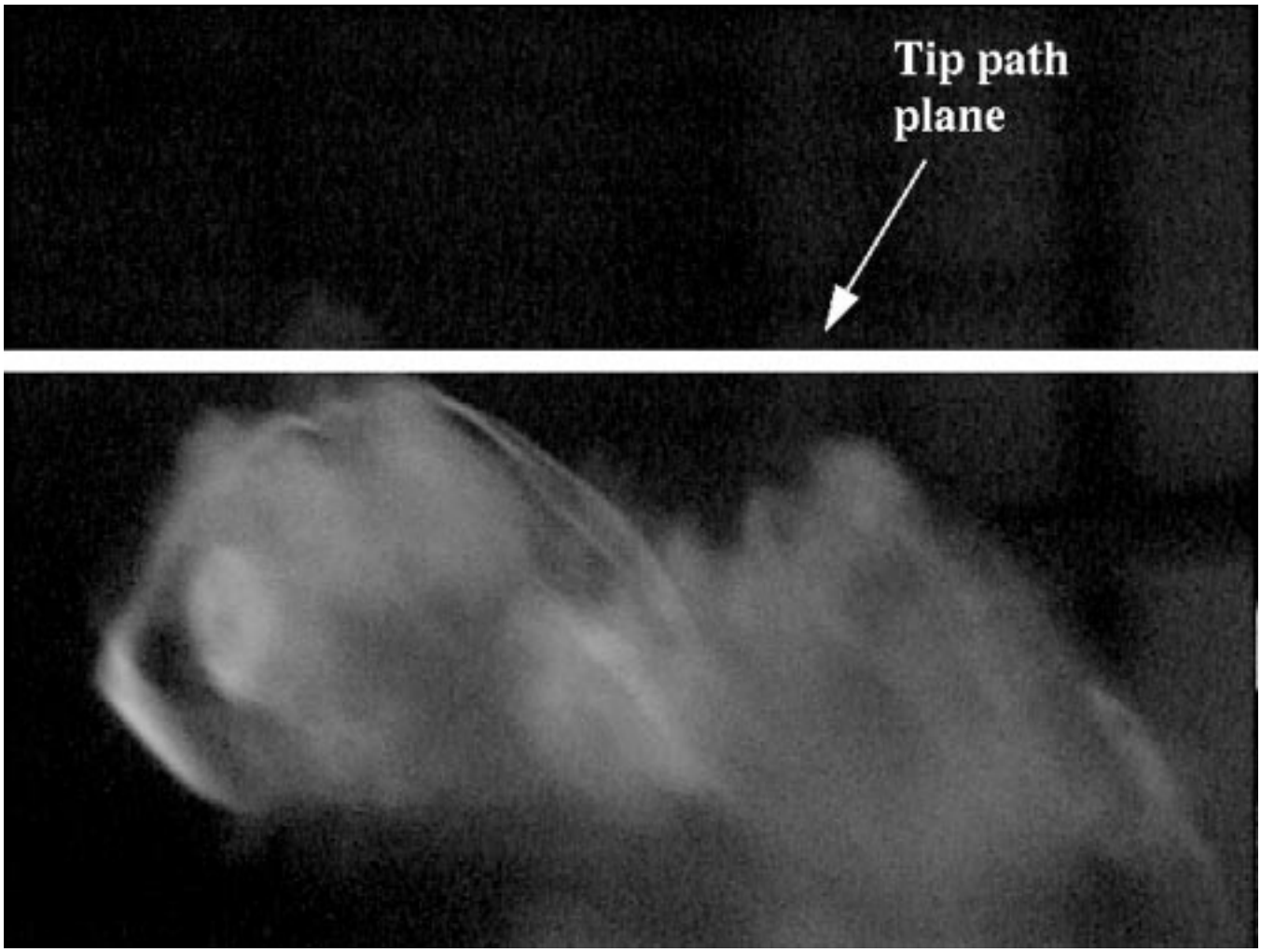

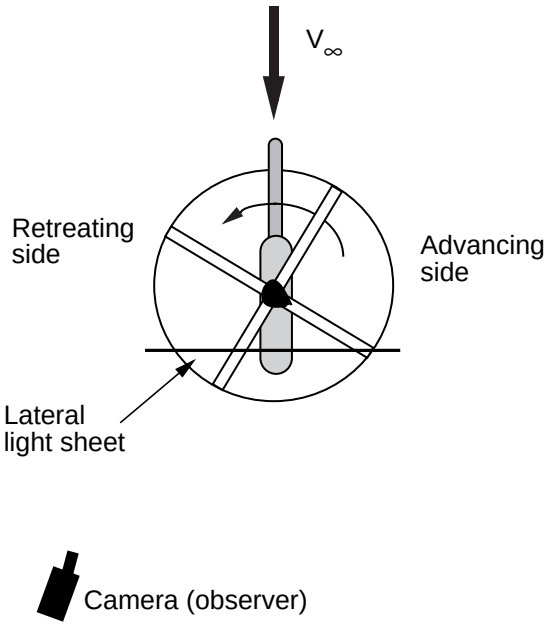

Figure 25. Lateral light sheet video image for station 7, under rotor plane, with μ = 0.10 and AMMS skewed −30°.

Figure 26. Wake from sight passing close to nose of helicopter, with $\mu = 0.10$ and AMMS skewed –30°.

REPORT DOCUMENTATION PAGE

Form Approved
OMB No. 0704-0188

1. AGENCY USE ONLY *(Leave blank)*	2. REPORT DATE	3. REPORT TYPE AND DATES COVERED
	March 1995	Technical Memorandum

4. TITLE AND SUBTITLE
Exploratory Flow Visualization Investigation of Mast-Mounted Sights in Presence of a Rotor

5. FUNDING NUMBERS
WU 505-59-36-01

PR 282-10-01-01

6. AUTHOR(S)
Terence A. Ghee and Henry L. Kelley

7. PERFORMING ORGANZATION NAME(S) AND ADDRESS(ES)
NASA Langley Research Center
Hampton, VA 23681-0001

Joint Research Program Office
Aeroflightdynamics Directorate
U.S. Army Aviation and Troop Command
NASA Langley Research Center
Hampton, VA 23681-0001

8. PERFORMING ORGANIZATION REPORT NUMBER
L-17409

9. SPONSORIING/MONITORING AGENCY NAME(S) AND ADDRESS(ES)
National Aeronautics and Space Administration
Washington, DC 20546-0001
and
U.S. Army Aviation and Troop Command
St. Louis, MO 63120-1798

10. SPONSORING/MONITORING AGENCY REPORT NUMBER
NASA TM-4634

ATCOM-TR-95-A-001

11. SUPPLEMENTARY NOTES
Ghee: Analytical Services & Materials, Inc., Hampton, VA; Kelley: JRPO, Aeroflightdynamics Directorate, ATCOM, Langley Research Center, Hampton, VA. This research was supported, in part, by the National Aeronautics and Space Administration under Contract No. NAS1-19831.

12a. DISTRIBUTION/AVAILABILITY STATEMENT
Unclassified–Unlimited
Subject Category 02
Availability: NASA CASI (301) 621-0390

12b. DISTRIBUTION CODE

13. ABSTRACT *(Maximum 200 words)*
A flow visualization investigation with a laser light sheet system was conducted on a 27-percent-scale AH-64 attack helicopter model fitted with two mast-mounted sights in the Langley 14- by 22-Foot Subsonic Tunnel. The investigation was conducted to identify aerodynamic phenomena that may have contributed to adverse vibration encountered during full-scale flight of the AH-64D Apache/Longbow helicopter with an asymmetric mast-mounted sight. Symmetric and asymmetric mast-mounted sights oriented at several skew angles were tested at simulated forward and rearward flight speeds of 30 and 45 knots. A laser light sheet system was used to visualize the flow in planes parallel to and perpendicular to the free-stream flow. Analysis of these flow visualization data identified frequencies of flow patterns in the wake shed from the sight, the streamline angle at the sight, and the location where the shed wake crossed the rotor plane. Differences in wake structure were observed between the sight configurations and various skew angles. Analysis of lateral light sheet plane data implied significant vortex structure in the wake of the asymmetric mast-mounted sight in the configuration that produced maximum in-flight vibration. The data showed no significant vortex structure in the wake of the asymmetric and symmetric configurations that produced no increase in in-flight adverse vibration.

14. SUBJECT TERMS
Helicopter; Mast-mounted sight; Flow visualization; Rotor

15. NUMBER OF PAGES
34

16. PRICE CODE
A03

17. SECURITY CLASSIFICATION OF REPORT	18. SECURITY CLASSIFICATION OF THIS PAGE	19. SECURITY CLASSIFICATION OF ABSTRACT	20. LIMITATION OF ABSTRACT
Unclassified	Unclassified	Unclassified	